International Journal of Rock Mechanics & Mining Sciences 171 (2023) 105581

Contents lists available at ScienceDirect

International Journal of Rock Mechanics and Mining Sciences

journal homepage: www.elsevier.com/locate/ijrmms

Permeability evolution and production characteristics of inclined coalbed methane reservoirs on the southern margin of the Junggar Basin, Xinjiang, China

Shun Liang [a,b,c,*], Yaowu Liang [a], Derek Elsworth [b], Qiangling Yao [a,b], Xuehai Fu [c], Junqiang Kang [b,c], Yisong Hao [a], Meng Wang [d]

[a] Key Laboratory of Deep Coal Resource Mining, Ministry of Education, School of Mines, China University of Mining and Technology, Xuzhou, Jiangsu, 221008, China
[b] EMS Energy Institute, G3 Center and Energy and Mineral Engineering, Pennsylvania State University, University Park, PA, 16802, USA
[c] Key Laboratory of CBM Resources and Reservoir Formation Process, Ministry of Education, China University of Mining and Technology, Xuzhou, Jiangsu, 221008, China
[d] School of Energy Science and Engineering, Henan Polytechnic University, Jiaozuo, Henan, 454003, China

ARTICLE INFO

Keywords:
Inclined coalbed methane reservoir
Asymmetric distribution
Coalbed methane
Permeability
Reservoir pressure

ABSTRACT

The thick and steeply inclined coal seams of the Junggar Basin of Xinjiang, China, are unique with dip angles generally >50° but over the range 0°–85°. Initial and evolving permeability and pressures change drastically around wells down-dip within the steeply inclined reservoir as a result of the depth differential. Hence, the evolution of permeability and fluid pressures during drainage exhibits significant differences from those of flat-lying or even slightly inclined reservoirs. We apply a hydro-mechanical model to evaluate the interaction of two-phase flows of gas and water in the inclined system. The influence of different reservoir inclinations (15°, 30°, 45°, 60°, and 75°) on the evolution of permeability, reservoir pressure, and gas production are explored through finite element modeling of this system. The results show that: 1) Reservoir inclination induces differences in permeability, reservoir pressure, gas content and methane production between the shallower updip reservoir and deeper downdip reservoir. The difference in permeability between the updip and downdip reservoirs is amplified as the dip angle increases and as drainage proceeds in the presence of the varying stress gradient. 2) An apparent asymmetric distribution of reservoir pressures results for wells along dip. The difference in reservoir pressure between the updip and downdip reservoirs intensifies as the inclination increases but lessens with the progress of drainage. The larger the dip angle, the smaller the final reservoir pressure. 3) The pressure reduction in the updip reservoir is larger than that in the downdip reservoir, resulting in the unsynchronized desorption of methane in the updip and downdip reservoirs. Methane within the updip reservoir desorbs preferentially over that in the downdip reservoir. For reservoir dip angles <45° a single peak in methane production rate is apparent but this is supplanted by dual peaks for inclinations >45°. The time gap in gas desorption between the updip and downdip reservoirs results in the "dual-peak" on gas production profile. 4) A larger well spacing along the dip of a more highly inclined reservoir results in more efficient water drainage and gas production. An inverted trapezoidal well pattern is recommended to facilitate the drainage and gas production of reservoirs with significant dip angles.

1. Introduction

Coalbed methane (CBM), within in coal seams and in both adsorbed and free states, is one important form of unconventional energy,[1–3] but it is also a greenhouse gas causes environmental pollution. In particular, large quantities of greenhouse gas are emitted during coal mining.[4] Hence, produce more secured energy to satisfy energy consumer and reduce greenhouse gas emissions is a major challenge facing many countries.[5–7] Global energy consumption has dramatically increased in past decades and is projected to keep increasing in the future.[8] CBM utilization can help supplement energy supply, cut greenhouse gas emissions and reduce risks in coal mining. There is abundant CBM

* Corresponding author. Room A601, School of Mines, China University of Mining and Technology, No.1 Daxue Rd., Xuzhou, Jiangsu Province, 221116, China.
E-mail address: 5756@cumt.edu.cn (S. Liang).

https://doi.org/10.1016/j.ijrmms.2023.105581
Received 23 March 2023; Received in revised form 24 July 2023; Accepted 4 September 2023
Available online 14 September 2023

resource in China, the total CBM resource located shallower than 2000 m is about 36.8 trillion m^3, ranking third in the world.[9,10] CBM reservoirs within China have various dip aspects. For example, strata dips within the Qinshui Basin range from 5° to 15°, those of the Sichuan Basin are in the range 15°–35°, while for the Junggar Basin in Xinjiang Province, which is a large superimposed basin dominated by Late Paleozoic and Mesozoic and Cenozoic continental deposits covering an area of 1.3×10^5 km^2,[11,12] are in the range 0°–90° and generally greater than 50°[13–18] (Fig. 1). This is obviously different from other basins in China and typical coal-bearing sedimentary basins abroad. Different reservoir dip angles impact the evolving permeability and reservoir pressures, resulting in significant differences in the recoverable gas resource, the choice of drainage technology, and wellbore layout from those for slightly inclined or flat-lying coal beds. Thus, the modes of exploitation of the huge CBM resource of the Junggar Basin, Xinjiang, China must be thoughtfully selected.[17,19]

Several multi-field and multi-phase physical models have been proposed to investigate the transport characteristics of gas and water in fractured coal seams. These include hydro-mechanical model (HM),[20] thermo-hydro-mechanical-chemical models (THMC),[21] a modified THMC model to increase the recovery of CBM through CO_2 injection (CO_2-ECBM),[22,23] and another THMC model to enhance the recovery rate of CBM through adjusting the acid pressure (AF-ECBM).[24] These models have offered suggestions to increase the permeability of the reservoir and to thereby enhance CBM production. When utilizing numerical simulation to evaluate CBM productivity, the reservoirs are commonly assumed to be horizontal because the encountered reservoirs in previous field CBM production are mainly horizontal or gently inclined (<15°).[25,26] In these studies, the effects of volumetric forces of water and gas (the buoyancy and gravity) are neglected since they are weak for flat-lying and slightly inclined reservoirs. However, significant differences exist in the drainage and gas production processes between steeply-dipping and shallowly inclined reservoirs. Gas and water within steeply inclined fractured reservoirs are more prone to segregate due to the effects of gravity and buoyancy.[27,28] Particularly, with increased inclination, the distribution of gas and water will have substantial variance between the updip and downdip reservoirs. Hence, the impact of reservoir inclination on the gas-water fluid system cannot be neglected. Some results and characteristics observed from previous studies in which the CBM reservoirs are set as flat-lying layers do not apply to the inclined reservoirs.[25,26] Gravity tends to exert opposite impacts on the transport of water in the updip and downdip reservoirs.[29–32] These effects, related to the stress gradient that is dependent on reservoir dip, result in significant differences in the evolution of permeability, reservoir pressure,[27] and gas production rate between the updip and downdip parts of the reservoir and within the drainage radius of a single well.[13–15,29] In different drainage stages, gas production is separately contributed from the updip and downdip parts of the reservoir and results in two peaks in the gas production rate profile.[13,15,33,34] In recent studies, it has been suggested that for steeply inclined

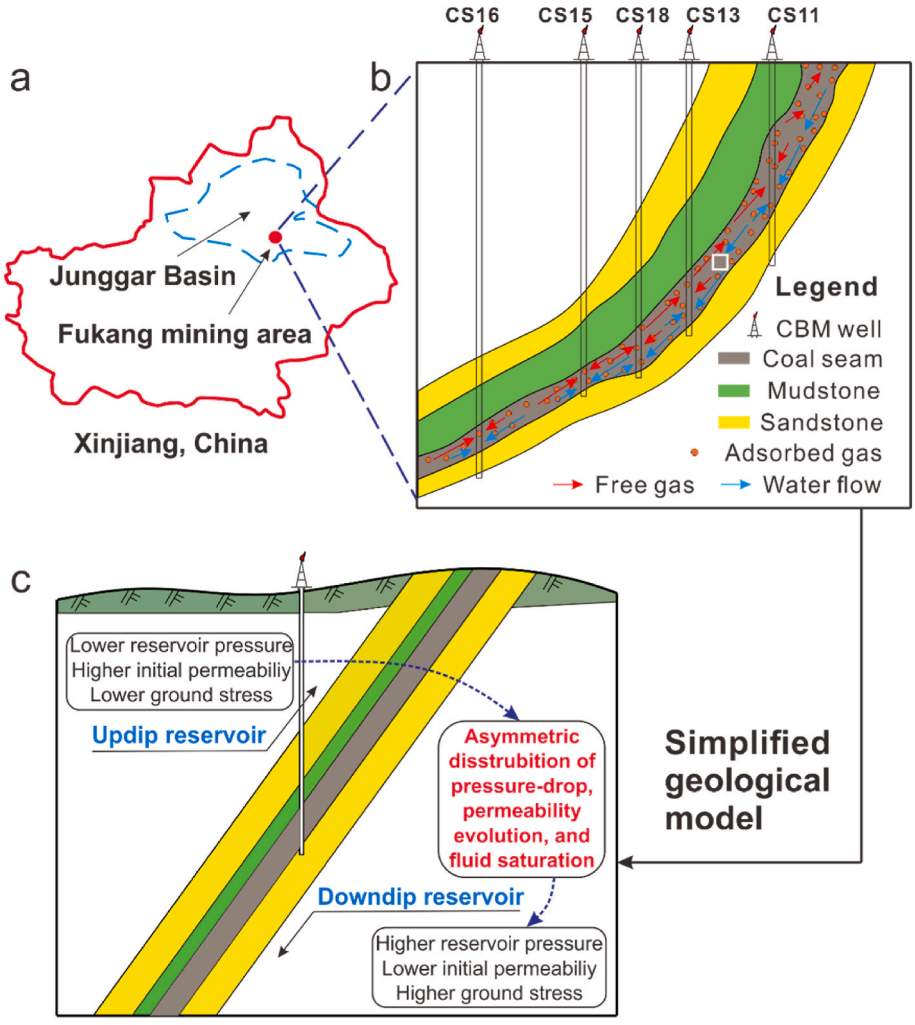

Fig. 1. Characteristics of steeply-dipping coalbed methane (CBM) reservoirs, (a) location of the study area in China, (b) characteristics of the coal seams in the Badaowan Formation of the west Fukang Block, (c) a simplified geological model of a steeply-dipping CBM reservoir. (modified from 15).

reservoirs, permeability along the strike could also be severely affected by coal matrix shrinkage, resulting in asymmetric evolution of the permeability relative to the well.[14,15] Thus, the influence of the deviatoric stress dependency of the reservoir dip on gas production cannot be ignored. Exploring the permeability evolution of reservoirs with different dip angles and identifying gas production characteristics is of great significance for optimizing wells layout and design of drainage process, which could also contribute to the recovery efficiency of inclined reservoirs.

Substantial studies have been conducted on reservoirs with limited or no inclination, but only a few studies have investigated the development of steeply inclined CBM reservoirs.[10,13,15,27,28,33–35] Some in-depth studies neglect the evolution of permeability, the reservoir pressure and the production capacity of CBM. Deep understanding of the impacts of volumetric forces of gas and water and stress gradient related with seam dip angle on the evolution of permeability, reservoir pressure, and gas production is rare, which restricts the efficiently commercial development of CBM in the Junggar Basin of Xinjiang, China. Based on previous studies,[20,36] a hydro-mechanical model considering the effects of gravity of water and buoyancy of gas is developed in this research. Influence of the stress gradient dependency of the reservoir dip on gas-water two-phase flow migration and gas production is emphasized. By analyzing the temporal and spatial evolution of reservoir pressure, permeability and gas production rate during gas drainage, the production characteristics of CBM in inclined reservoirs is revealed. This work contributes to the efficient recovery of the rich CBM resource of the inclined reservoirs on the southern margin of the Junggar Basin, Xinjiang, China.

2. The coupling model for CBM development in inclined coal seams

In the process of drainage and gas production, the change of effective stress and gas desorption leads to coal deformation, with feedbacks on coal permeability. Based on previous studies,[20–22,24] we establish a coupling model incorporating the effects of water and gas for inclined CBM reservoirs. This model includes control of coal deformation on the stress field, the governing equations of gas-water two-phase flow migration and coupling with changes in porosity and permeability. Such couplings more faithfully reflect changes in gas and water migration, reservoir pressure, effective stress and permeability caused by their coupling in the process of CBM drainage and production, with specific application to inclined reservoirs.

2.1. Basic assumptions of the model

According to the characteristics of fracture and pore structure and gas adsorption/desorption behavior of coal reservoirs, the following assumptions are adopted.[14,20–22,37–43]

1) The coal reservoir is a single-permeability (fracture) poroelastic continuum with dual-porosity (fractures/cleats and micro-pores in the matrix);
2) Methane is treated as an ideal gas, which exists and migrates in both the matrix pores and fractures of coal reservoir in adsorbed and free state, while water only exists and migrates within fractures of the coal reservoir;
3) The CBM and water saturate the entire matrix and fractures, and the dynamic process of adsorption/desorption of CBM in the matrix satisfies the Langmuir isotherm adsorption equation;
4) The CBM desorbs and is transported from matrix to fractures by diffusion (Fick's law) and migrates along fractures by Darcian flow.

The general interactions between methane and water in the CBM reservoir are shown schematically in Fig. 2.

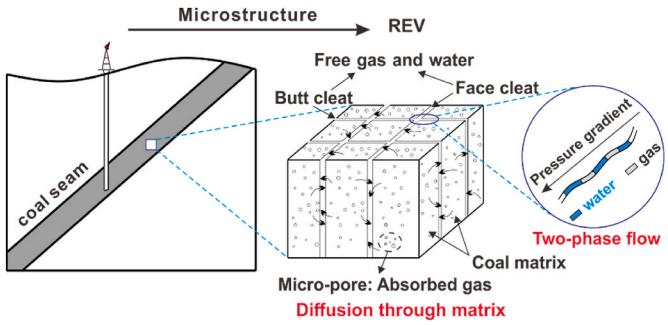

Fig. 2. Methane and water migration mechanisms in steeply-dipping coal seams.

2.2. Governing equations

2.2.1. Governing equation of coal deformation

The coal reservoir is represented as an elastic continuum with double porosity but single permeability, representing the fracture network. The mechanical characteristics are modulated by the presence of fractures and matrix pores. Based on the Navier equation, considering gas pressure and gas adsorption/desorption in matrix and fractures, the governing equation for stresses within the coal reservoir are defined as:[20,22,44–47]

$$\varepsilon_{ki}=\frac{1}{2G}\sigma_{ki}-\left(\frac{1}{6G}-\frac{1}{9K}\right)\sigma_{ll}\delta_{ki}+\frac{1}{3}\varepsilon_s\delta_{ki}+\frac{1}{3K}\left(\alpha_m p_{mg}+\alpha_f p_f\right)\delta_{ki} \tag{1}$$

where ε_{ki} is the strain tensor (k, i = 1, 2, 3); G is the shear modulus, $G = D/(1+\nu)$, Pa; K is bulk modulus of the coal, $K = D/3$ (1-2ν), Pa; ν is Poisson's ratio of the coal; D is the effective elastic modulus, Pa, $D = 1/[1/E + 1/L_m K_n]$, in which E is the Young's modulus of the coal, L_m is the width of the matrix, m, and K_n is the normal stiffness of the fracture, Pa/m; ε_s is the volume strain within the matrix caused by gas adsorption/desorption,[43] which is fitted onto Langmuir-type curves and has been verified through experiments.[48,49] The Langmuir-type equation can be expressed as:[43,50] $\varepsilon_s = \varepsilon_l p_m/(p_l + p_m)$, in which ε_l is the Langmuir-type strain coefficient, representing the maximum adsorption-induced strain; p_l is the Langmuir gas pressure constant, Pa; and p_m is the gas pressure in the matrix, Pa. δ_{ki} in Eq. (1) is the Kronecker delta with 1 for $k = i$ and 0 for $k \neq i$; σ_{ki} is the total stress tensor, and σ_{ll} is the normal stress component, $\sigma_{ll} = \sigma_{11}+\sigma_{22}+\sigma_{33}$; α_m is Biot effective stress coefficient for the matrix, $\alpha_m = 1 - K/K_S$, K_S represents the bulk modulus of the coal grains, Pa;[50–52] α_f is Biot effective stress coefficient for the fracture network, $\alpha_f = 1 - K/K_f = 1 - K/(L_m K_n)$;[50–52] p_{mg} is the gas pressure in the matrix, Pa; p_f is the total fluid pressure within the fractures, including gas pressure and water pressure, $p_f = s_g p_{fg} + s_w p_{fw}$, Pa; s_g is gas phase saturation, s_w is water phase saturation, $s_g + s_w = 1$; and, p_{fg} is the gas pressure in the fractures, Pa; p_{fw} is the water pressure in the fractures, Pa.

The deformation-strain and stress equilibrium relationships for the coal reservoir can be expressed as follows:

$$\varepsilon_{ki}=\frac{1}{2}\left(u_{k,i}+u_{i,k}\right) \tag{2}$$

$$\sigma_{ki,i}+F_k=0 \tag{3}$$

where u_k is displacement in the k-direction, m; F_k is the body force in the k-direction, N.

Combining Eqs. (1)–(3), the governing equation for the combined deformation and stress field within the coal reservoir is defined as:

$$\underbrace{Gu_{k,ii}+\frac{G}{1-2v}u_{i,ik}}_{\text{Ground stress}}-\underbrace{(\alpha_m p_{m,k}+\alpha_f p_{f,k})}_{\text{Mixture fluid pressure in matrix and fracture}}-\underbrace{K\varepsilon_{s,k}}_{\text{Gas adsorption or desorption induced stress}}+F_k=0 \tag{4}$$

2.2.2. Governing equations of gas-water two-phase flow

The pores and fractures within the coal reservoir are saturated with a mixture of gas and water. The gas migrates both in the coal matrix and fractures, while only water is transported in the fractures. The transfer of methane from coal matrix to fractures occurs in two steps: first, the adsorbed gas desorbs from the surface of the pores in the coal matrix, diffuses through the bulk matrix then flows into and through the fractures/cleats. This process obeys Fick's and Darcy's laws, and the transportation of gas and water in coal fractures obeys Darcy's law.

The diffusion of methane from coal matrix to fractures can be expressed as:[14,20,53,54]

$$\frac{\partial m_g}{\partial t}=-\frac{3\pi^2 D_i}{L^2}\cdot\frac{M_g}{RT}\left(p_{mg}-p_{fg}\right) \tag{5}$$

where m_g is the mass of gas in the matrix, kg; M_g is the molar mass of methane, kg/mol; R is the molar constant of methane, J/(mol·K); T is the temperature of coal reservoir, K; D_i is the gas diffusion coefficient, m^2/s; and L is the cleat spacing, m.

The gas in coal reservoir matrix contains both adsorbed gas and free gas, so the mass of gas in the matrix can be expressed as:[22,55,56]

$$m_g=\rho_s\frac{M_g}{RT_s}p_s\cdot\frac{V_L p_{m_g}}{P_{m_g}+P_L}+\varphi_m\frac{M_g}{RT}p_{m_g} \tag{6}$$

where ρ_s is the matrix density of the coal reservoir, kg/m^3; T_s is the reservoir temperature under standard conditions, K; p_s is standard atmospheric pressure, Pa; V_L is the Langmuir volume constant; P_L is the Langmuir pressure constant; and φ_m is the porosity of coal matrix.

By substituting Eq. (6) into Eq. (5), the governing equation for CBM migration in the coal reservoir matrix is as follows:

$$\frac{\partial}{\partial t}\left(\underbrace{\rho_s\frac{M_g}{RT_s}p_s\cdot\frac{V_L p_{m_g}}{P_{m_g}+P_L}}_{\text{Adsorbed gas}}+\underbrace{\varphi_m\frac{M_g}{RT}p_{m_g}}_{\text{Free gas}}\right)=-\frac{3\pi^2 D_i}{L^2}\cdot\frac{M_g}{RT}\left(p_{mg}-p_{fg}\right) \tag{7}$$

Free methane may be present within fractures. The governing equations controlling gas and water migration in coal reservoir fractures can be obtained from mass conservation as:[21,22,57]

$$\frac{\partial}{\partial t}\left(s_g\frac{M_g p_{fg}}{RT}\varphi_f\right)+\nabla\bullet\left[-\frac{M_g\left(p_{fg}+b\right)}{RT}\frac{k_f k_{rg}}{\mu_g}\left(\nabla p_{fg}+\rho_g g\nabla z\right)\right]=\left(1-\varphi_f\right)\frac{3\pi^2 D_i}{L^2}\cdot\frac{M_g}{RT}\left(p_{mg}-p_{fg}\right) \tag{8}$$

$$\frac{\partial}{\partial t}\left(s_w\rho_w\varphi_f\right)+\nabla\bullet\left[-\rho_w\frac{k_f k_{rw}}{\mu_w}\left(\nabla p_{fw}+\rho_w g\nabla z\right)\right]=0 \tag{9}$$

where φ_f is the fracture porosity of the coal reservoir; b is the Klinkenberg factor, Pa; k_f is the fracture permeability of the coal reservoir, m^2; k_{rg} is the relative permeability of gas; k_{rw} is the relative permeability of water; μ_g is the gas dynamic viscosity, and μ_w is the water dynamic viscosity; ρ_g and ρ_w are the gas density and water density, respectively, kg/m^3; ∇z is the gravitational term.

The relative permeability to methane and water can be expressed as:[58,59]

$$k_{rg}=\left[1-\left(\frac{s_w-s_{wr}}{1-s_{gr}-s_{wr}}\right)\right]^2\bullet\left[1-\left(\frac{s_w-s_{wr}}{1-s_{wr}}\right)^2\right] \tag{10}$$

$$k_{rw}=\left(\frac{s_w-s_{wr}}{1-s_{wr}}\right)^4 \tag{11}$$

where s_{wr} is the irreducible water saturation, s_{gr} is the residual gas saturation.

2.2.3. Permeability coupling equation

In coal reservoirs, permeability and porosity respond to coal deformation with this impacting gas-water two-phase transport. Fracture porosity of the coal reservoir can be expressed as:[43,57]

$$\frac{\varphi_f}{\varphi_{f0}}=1+\frac{\Delta L_f}{L_{f_0}} \tag{12}$$

where L_f is the aperture of fracture in coal mass, and the subscript "0" denotes the initial value of the corresponding variables.

The change in effective stress results from the sorption effect. Since a change in effective stress results the corresponding fracture dilation can be obtained as:[43,57]

$$\Delta L_f=-\frac{L_{f0}}{K_f}\cdot\frac{1}{A}\left(\Delta\varepsilon_s-\Delta\varepsilon_v\right) \tag{13}$$

where ΔL_f is fracture aperture change; $A=\frac{L_{f0}}{L_m K_f}+\frac{1}{K}$; K_f is the modified fracture stiffness, $K_f=L_m K_n$, L_m is the width of the matrix, m, and K_n is the fracture stiffness, Pa/m; $\Delta\varepsilon_s$ and $\Delta\varepsilon_v$ are the swelling strain and volumetric strain of coal mass induced by gas adsorption, respectively. According to the previous studies,[43,50,60–62] $\varphi_{f0}=\frac{3L_{f0}}{L_m}$.

Experiments show that the permeability of the coal fracture k_f varies with porosity and is denoted as follows:[63,64]

$$\frac{k_f}{k_{f0}}=\left(\frac{\varphi_f}{\varphi_{f0}}\right)^3 \tag{14}$$

Substitute Eqs. (12) and (13) into Eq. (14), then the fracture permeability can be expressed as:

$$\frac{k_f}{k_{f0}}=\left[1-\frac{3}{\varphi_{f0}+3K_f/K}\left(\Delta\varepsilon_s-\Delta\varepsilon_v\right)\right]^3 \tag{15}$$

Eqs. (4), (8), (9) and (15) define coupled coal deformation and migration of gas-water two-phase flow in dual-porosity media. In the hydro-mechanical model, the governing equations are nonlinear second-order partial differential equations (PDEs) in space and first-order PDEs in time. These equations cannot be theoretically and analytically solved because of the nonlinearity in both the space and time domains.[44,65] Therefore, we implement these coupled equations into solid mechanics and PDE modules of the finite element software - COMSOL Multiphysics to evaluate the interaction of two-phase flows of gas and water in the inclined system via the discrete and finite-element method. The solid mechanics module is used to describe Eq. (4) and the gas-water two-phase flow in the fracture system are represented by the PDE modules (Eqs. (7)–(9)).

To concisely illustrate the research flow of work in this study, a chart is presented as below (Fig. 3).

2.3. Parameters in the coupling model

A simplified physical model is established to appropriately represent the field conditions. The model size is 300 m × 300 m × 5 m. The drainage well is located in the middle of the coal seam, with a diameter of 0.2 m and the bottom hole depth of 800 m, and the thickness of the coal seam is 5 m. Five scenarios are developed with different coal seam dip angles of 15°, 30°, 45°, 60°and 75°. The coal seam burial depth ranges from 655.1 m to 944.9 m. According to the average volume weight of the overlying strata above the coal seam under the above five different coal seam dip angle conditions, an equivalent load is applied to

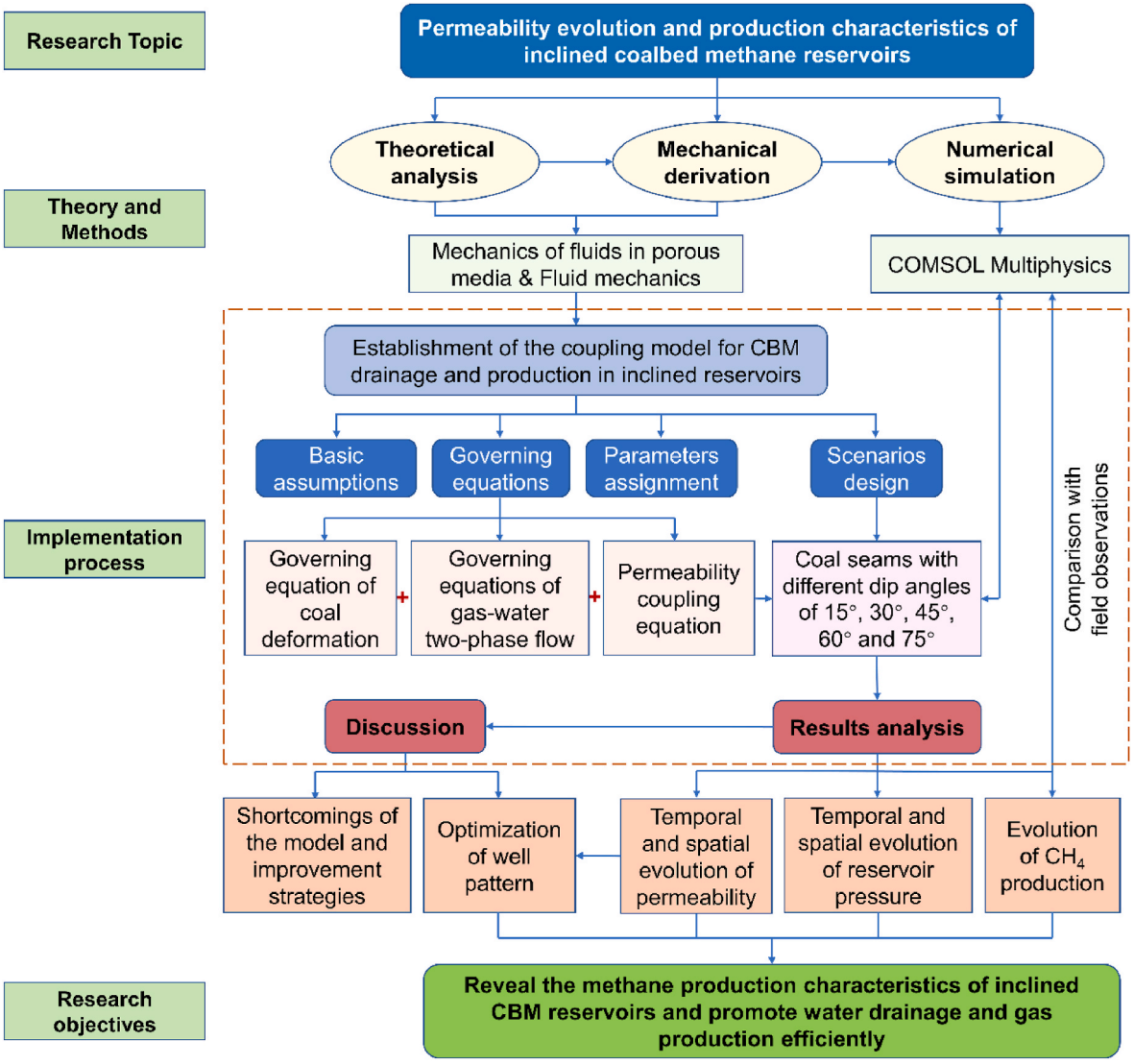

Fig. 3. The research flow chart of this study.

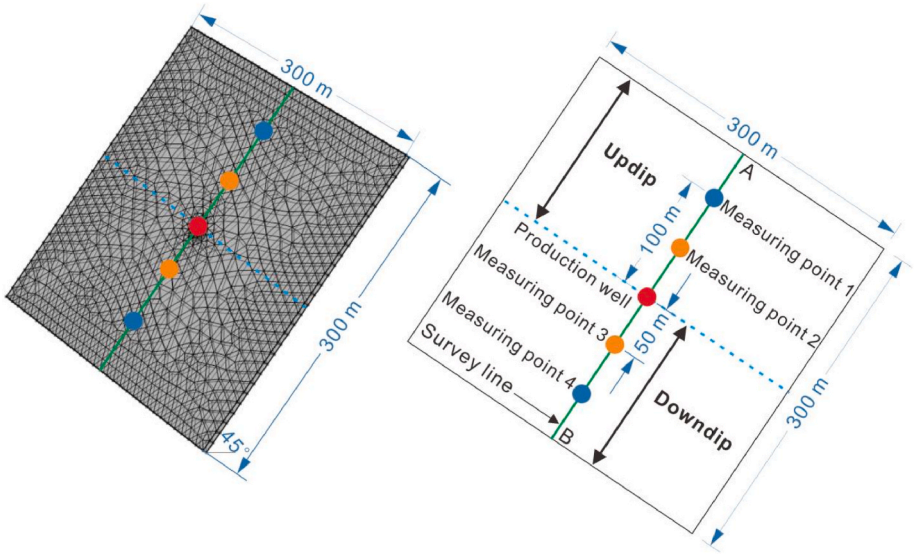

Fig. 4. Meshed coalbed for simulation (taking a dip inclination of 45° as an example).

the upper boundary of the model. The borders around and at the bottom of the model are fixed. All external boundaries are insulated and impermeable to methane and water. Therefore, under initial conditions, the coal seam is considered to be in a free stress state, and the initial reservoir pressure is determined by the reservoir pressure gradient. The model is divided into grid of free triangles, with a transect AB traversing the center of the model along the dip and containing two groups of symmetrical monitoring points (points 1 and 4, and points 2 and 3) respectively 50 m (points 2 and 3) and 100 m (points 1 and 4) from the drainage well (Fig. 4, taking the dip angle 45° as an example). Table 1 defines the basic geomechanical parameters for the coupled model, which as derived from field data and relevant research literature.[14,21,36,66]

3. Results and analysis

3.1. Temporal and spatial evolution of permeability in reservoirs of various inclinations

During the process of drainage and gas production the permeability is controlled jointly by effective stress and the desorption of methane. In the initial stage of drainage, the coal reservoir mainly produces water with the effect of reducing water pressure, increasing effective stress and compacting voids within the coal matrix. As water drainage proceeds, the positive effect of increase in permeability due to matrix shrinkage and caused by methane desorption ultimately overwhelms the counter effect of increased effective stress – this results in the net swelling of voids in the matrix. As a result of this, permeabilities in reservoirs of different dips first decrease and then increase (Fig. 5). Different degrees of asymmetric evolution in permeability result at symmetrically disposed updip and downdip measuring locations. For coal reservoirs with different inclinations (scenarios 1 to 5 representing dips inclinations of 15°–75°) the difference in the permeability ratio (k/k_0) at 2200 days, between the upper (point 1) and lower (point 2) measuring locations within the updip coal reservoir (the permeability ratio of point 2 minus that of point 1) were 0.01, 0.01, 0.01, 0.01, and 0.03 respectively. However, the difference-value in the ratio (k/k_0) between the upper measuring location (point 3) and the lower measuring location (point 4) within the downdip coal reservoir (the permeability ratio of point 3 minus that of point 4) were higher as 0.02, 0.03, 0.05, 0.06, and 0.09 respectively. The difference-values in the downdip permeability ratios (k/k_0) are clearly greater than those in the updip direction, indicating a greater variance in permeability along the downdip leg of the reservoir.

For reservoirs at various inclinations, the drawdown time for permeability ratio to reach its lowest value (the duration from the initial value of the permeability ratio to the lowest value) at measuring point 1 was observed on drainage days 1005, 918, 786, 612, and 376, respectively. The recovery time to then climb from this minimum permeability ratio back to $k/k_0 = 1$ was 1915, 1633, 1342, 1032, and 659 days of drainage. The detailed timeline of the drawdown and recovery is presented in Tables 2 and 3 for measuring points 2 (above) and 3 and 4 (below drainage well). It is worth mentioning that the permeability at measuring point 4 failed to recover for inclinations of 15°, 30°, and 45°. The recovery of permeability at inclinations of 60° and 75° occurred on days 2192 and 1637 of drainage. The comparison between permeability drawdown and recovery times reveals that the drawdown time for the permeability tends to decrease with increasing inclination. Closer distances from the production well return a shorter rebound time and a greater recovery in the permeability. Compared with the downdip limb of a reservoir, the updip limb demonstrates shorter drawdown and recovery times (Tables 2 and 3, and Fig. 5) reflecting the impacts of reduced in situ effective stresses at shallower depths and potentially larger changes in pressure driven by gravity drainage.

The permeability drawdown then recovery is mainly caused by the effective stresses and the matrix shrinkage under the desorption of methane. Water drainage and methane production tend to increase the effective stresses, resulting in a reduction in permeability. While the desorption of methane leads to shrinkage of the matrix, resulting in an increase in permeability. The differences in the updip and downdip direction affect the drainage, resulting in variances in the separation of gas and water. Lower inclinations are often accompanied with slower downward water drainage and limited gas and water separation. Higher inclinations, on the other hand, often accelerate the drainage and results in more severe gas and water separation. In practice, the spacing between wells along the dip of reservoirs with varying inclinations should be discreetly selected according to the effective reach of a single well. A larger well spacing along the dip of a more highly inclined reservoir might result in more efficient water drainage and gas production.

We define the ratio, equal to the maximum absolute permeability divided by the minimum permeability during drainage within the updip/downdip limb of the reservoir, as the permeability difference factor of the updip/downdip reservoir. This factor may be used to evaluate the asymmetric development of permeability between the updip and downdip reservoirs. For reservoirs with various inclinations (scenarios 1–5), at the initial stage (on drainage day 0), the permeability difference factors were identified as 1.36, 1.81, 2.32, 2.80, and 3.17, which changed into 1.31, 1.71, 2.13, 2.46, and 2.49 on production day 1000, 1.28, 1.67, 2.08, 2.39, and 2.44 on production day 1500, and then 1.27, 1.64, 2.04, 2.35, and 2.40 after 2000 days of drainage (Table 4 and Fig. 6). The permeability difference factor on the updip limb of the reservoir tends to increase with inclination, which decreases as drainage and gas production proceed. It is surmised that gravity drainage is enhanced for greater inclinations of the updip part of the reservoir, resulting in a greater permeability difference factor. However, as drainage and gas production proceed, the negative effect of decreased permeability with increased effective stress is suppressed by the positive effect of matrix shrinkage. Therefore, the difference factor of the updip limb of the reservoir tends to decrease with gas production.

In the downdip direction of the seam, and initially (drainage day 0), the permeability difference factors were identified as 1.36, 1.81, 2.31, 2.79, and 3.15, which changed to 1.77, 2.47, 3.47, 5.03, and 7.17 on production day 1000, 1.84, 2.56, 3.61, 5.21, and 7.15 on production day 1500, and 1.90, 2.65, 3.69, 5.29, and 7.08 after 2000 days of drainage (Table 5 and Fig. 7). Similar to the updip part, the permeability difference factor in the downdip part also tends to increase with growing inclination. It is worth mentioning that the permeability difference factor at inclinations of 15°, 30°, 45°, and 60° tends to increase as gas production proceeds. When the reservoir inclination reaches 75°, the

Table 1
Parameters in the numerical simulation model.

Parameters	Values and Units	Parameters	Values and Units
Desorption time τ	8.71 d	Langmuir pressure constant P_L	3.034 MPa
Young's modulus of coal E	3000 MPa	Langmuir volume constant V_L	0.036 m^3/kg
Poisson's ratio of coal ν	0.3	The density of coal skeleton ρ_c	1400 kg/m^3
Initial porosity of coal matrix φ_{m0}	0.045	Rock density ρ_r	2500 kg/m^3
Initial porosity of fracture φ_{f0}	0.005	Pumping negative pressure p_c	0.201 MPa
Capillary pressure p_{cgw}	0.05 MPa	Initial water saturation S_{w0}	0.8
Gas dynamic viscosity μ_g	1.03×10^{-5} Pa s	Initial gas saturation S_{g0}	0.2
Water dynamic viscosity μ_w	1.01×10^{-3} Pa s	Biot effective stress coefficient for the coal matrix α_m	0.99436
fracture stiffness K_n	4.8 GPa	Biot effective stress coefficient for the fracture network α_f	0.17136

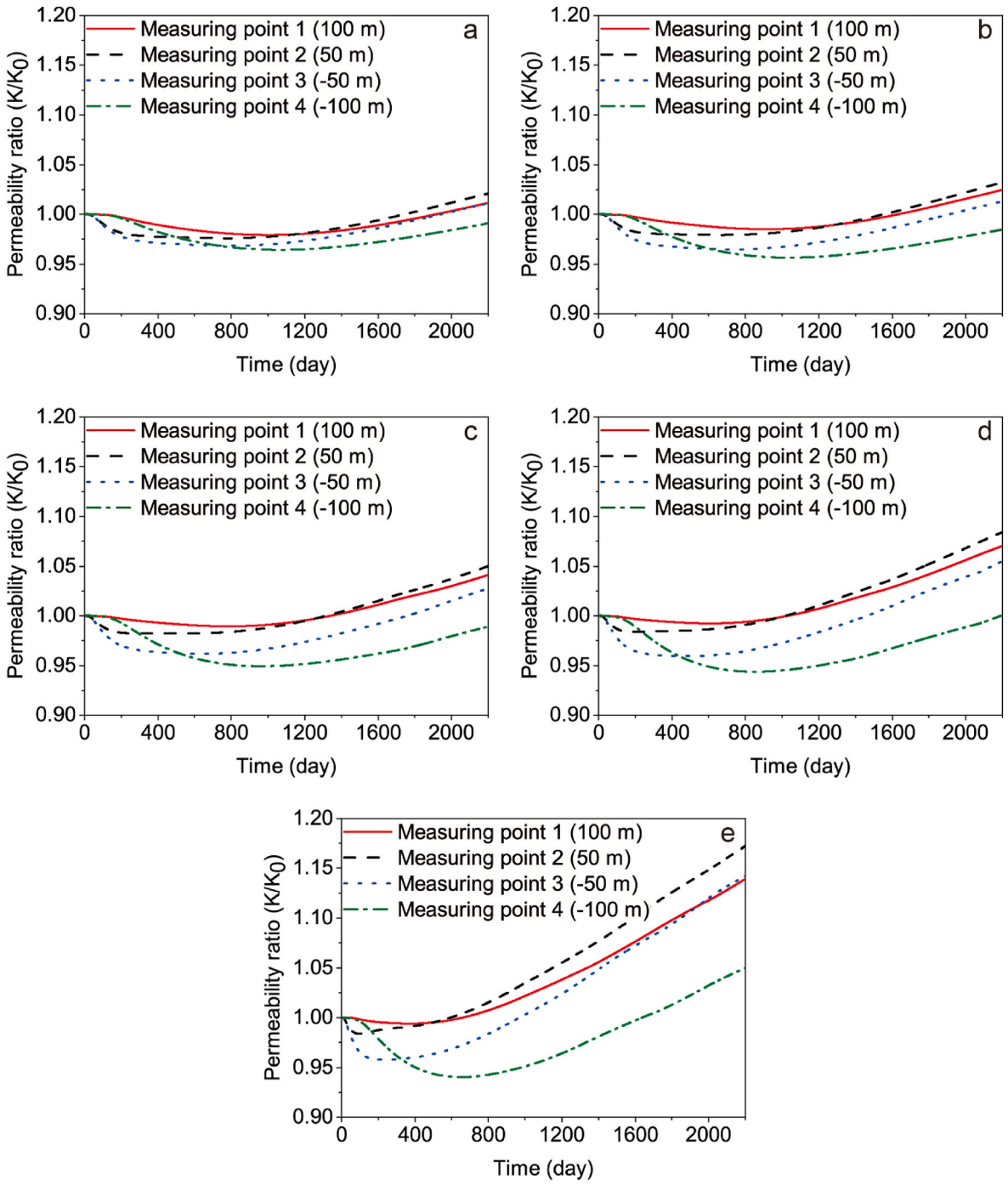

Fig. 5. Permeability ratio at various measuring locations for coal reservoirs with different inclinations (a-15°, b-30°, c-45°, d-60°, e–75°).

Table 2
Rebound time (day) for the permeability ratio at four measuring points for coal reservoirs with different inclinations.

Measuring point	The dip angle of the reservoir				
	15°	30°	45°	60°	75°
1	1005	918	786	612	376
2	759	671	513	193	101
3	786	734	639	487	229
4	1063	1035	969	853	653

Table 3
Recovery time (day) for the permeability ratio at four measuring points for coal reservoirs with different inclinations.

Measuring point	The dip angle of the reservoir				
	15°	30°	45°	60°	75°
1	1915	1633	1342	1032	659
2	1744	1556	1317	1019	595
3	1942	1911	1758	1464	970
4	–	–	–	2192	1637

Table 4
Permeability difference factors for the updip part of the reservoir for different inclinations after different production times.

Production time (day)	The dip angle of the reservoir				
	15°	30°	45°	60°	75°
0	1.36	1.81	2.32	2.80	3.17
1000	1.31	1.71	2.13	2.46	2.49
1500	1.28	1.67	2.08	2.39	2.44
2000	1.27	1.64	2.04	2.35	2.40

permeability difference factor of the downdip part of the reservoir first increases and then decreases as gas production proceeds. As drainage proceeds, effective stress impacts dominate the preliminary drainage stage, resulting in an increase in the permeability difference factor of the downdip reservoir. However, at the later stage of drainage, less water remains and drainage slows. Gas desorption effects overpower the permeability reduction effects of increased effective stress, resulting in a reduction in permeability difference factor in the downdip part of the reservoir.

Similarly, the ratio between the peak absolute permeability in the updip part of the reservoir and the minimum absolute permeability in the downdip part of the reservoir is defined as the permeability difference factor of the entire reservoir. This ratio could be adopted to evaluate the asymmetric difference in permeability between the updip and downdip portions of the reservoir. For reservoirs with various inclinations (15°, 30°, 45°, 60°, 75°), at the initial stage (day 0), the permeability difference factors were identified as 1.86, 3.30, 5.42, 7.92, and 10.10 respectively, which changed to 1.90, 3.47, 5.82, 8.63, and 11.21 on production day 1000, and then 1.91, 3.48, 5.86, 8.75, and 11.36 on production day 1500, and finally to 1.92, 3.50, 5.86, 8.77, and 11.50 after production for 2000 days (Table 6, Figs. 6 and 7). Clearly, the permeability difference factor of the entire inclined reservoir increases as the inclination grows and as production proceeds. This indicates that the permeability across the entire reservoir is affected by both the inclination and drainage time. Steeply inclined reservoirs better favor water drainage, resulting in a larger reservoir pressure drop and larger changes in effective stress together with an asymmetric distribution of the permeability with regard to the drainage well.

Table 5
Permeability difference factor for the downdip portion of reservoirs with different inclinations after different production times.

Production time (day)	The dip angle of the reservoir				
	15°	30°	45°	60°	75°
0	1.36	1.81	2.31	2.79	3.15
1000	1.77	2.47	3.47	5.03	7.17
1500	1.84	2.56	3.61	5.21	7.15
2000	1.90	2.65	3.69	5.29	7.08

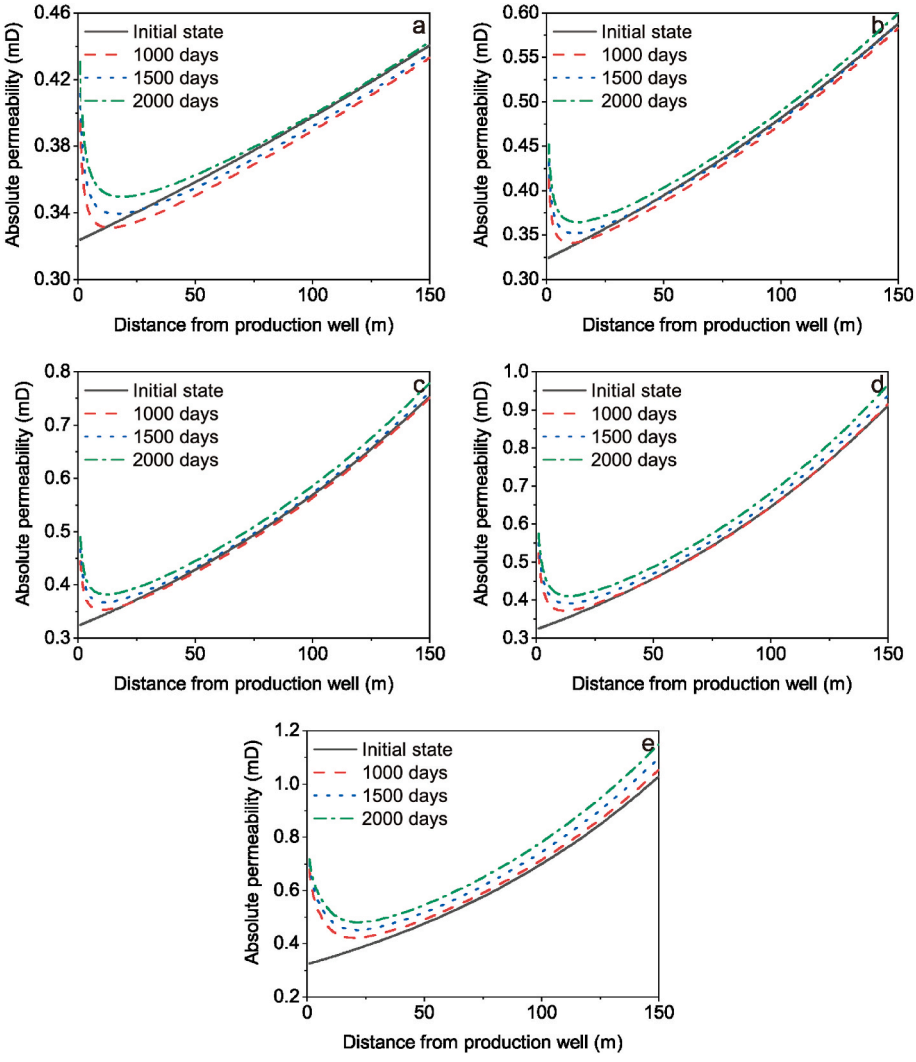

Fig. 6. Evolution of absolute permeability in the updip part of reservoirs with varying inclinations (a-15°, b-30°, c-45°, d-60°, e–75°).

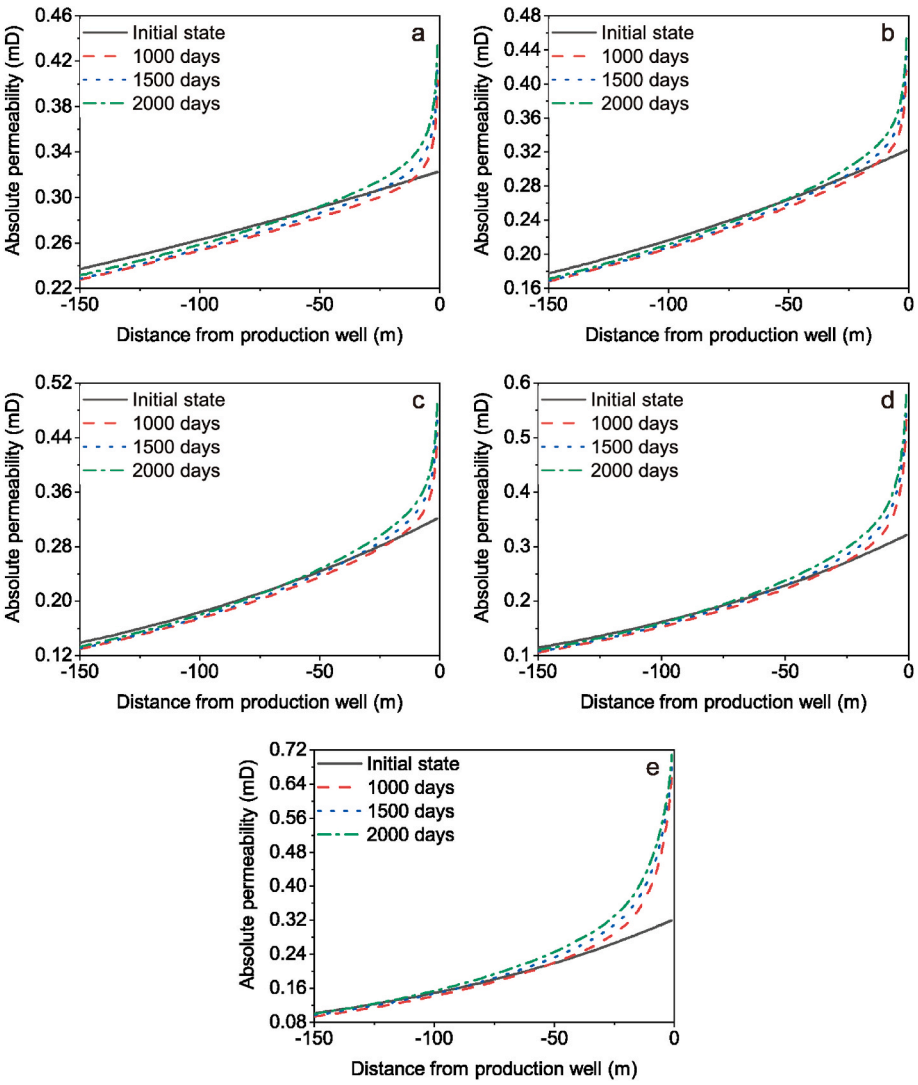

Fig. 7. Evolution of absolute permeability in the downdip part of reservoirs with different inclinations (a-15°, b-30°, c-45°, d-60°, e–75°).

Table 6
Permeability difference factors for reservoirs with different inclinations after different production times.

Production time (day)	The dip angle of the reservoir				
	15°	30°	45°	60°	75°
0	1.86	3.30	5.42	7.92	10.10
1000	1.90	3.47	5.82	8.63	11.21
1500	1.91	3.48	5.86	8.75	11.36
2000	1.92	3.50	5.86	8.77	11.50

According to the above analysis, in the updip reservoir, the permeability difference factor decreases with drainage and gas production. In the downdip reservoir, the difference factor increases with drainage and gas production. However, the permeability difference factor for the entire reservoir also increases as gas production proceeds, indicating that the permeability changes more in the downdip reservoir, which dominates the permeability evolution of the entire reservoir.

3.2. Temporal and spatial evolution of reservoir pressure in inclined reservoirs

The reservoir pressure often refers to the total fluid pressure in the fracture of the coal seam, including both gas and water pressures. As demonstrated in Fig. 8, the pressure for reservoirs with different inclinations varies as the drainage and gas production proceed. The asymmetric character of the reservoir pressure distribution is identified between the updip and downdip reservoirs. The largest difference in reservoir pressure between the updip and downdip reservoirs is exhibited after production for 1000 days. The greater the dip angle, the more obvious this asymmetry of the pressure distribution. Under gravity, the drainage is facilitated within the updip part of the reservoir, but is suppressed within the downdip part. This results in the reservoir pressure in the downdip part of the reservoir always being greater than that in the updip reservoir.

Fig. 9 shows resulting changes in reservoir pressure of seams with dip angles of 15°, 45°, and 75° from production day 400–2000. Clearly, an increase in inclination leads to a greater pressure difference between the updip and downdip reservoirs. As water drainage and gas production proceed, the pressure distribution difference between the updip and downdip reservoirs all become smaller for reservoirs with different dip angles. Furthermore, a greater inclination returns a lower final reservoir pressure across the entire seam, indicating improved performance in drainage and gas production.

Fig. 10 displays changes in reservoir pressure of seams with various dip angles (from 15° to 75°) as gas production proceeds. Due to the effects of gravity and water drainage, the pressure in the updip and downdip reservoirs drops quickly, followed by a slower rate of pressure

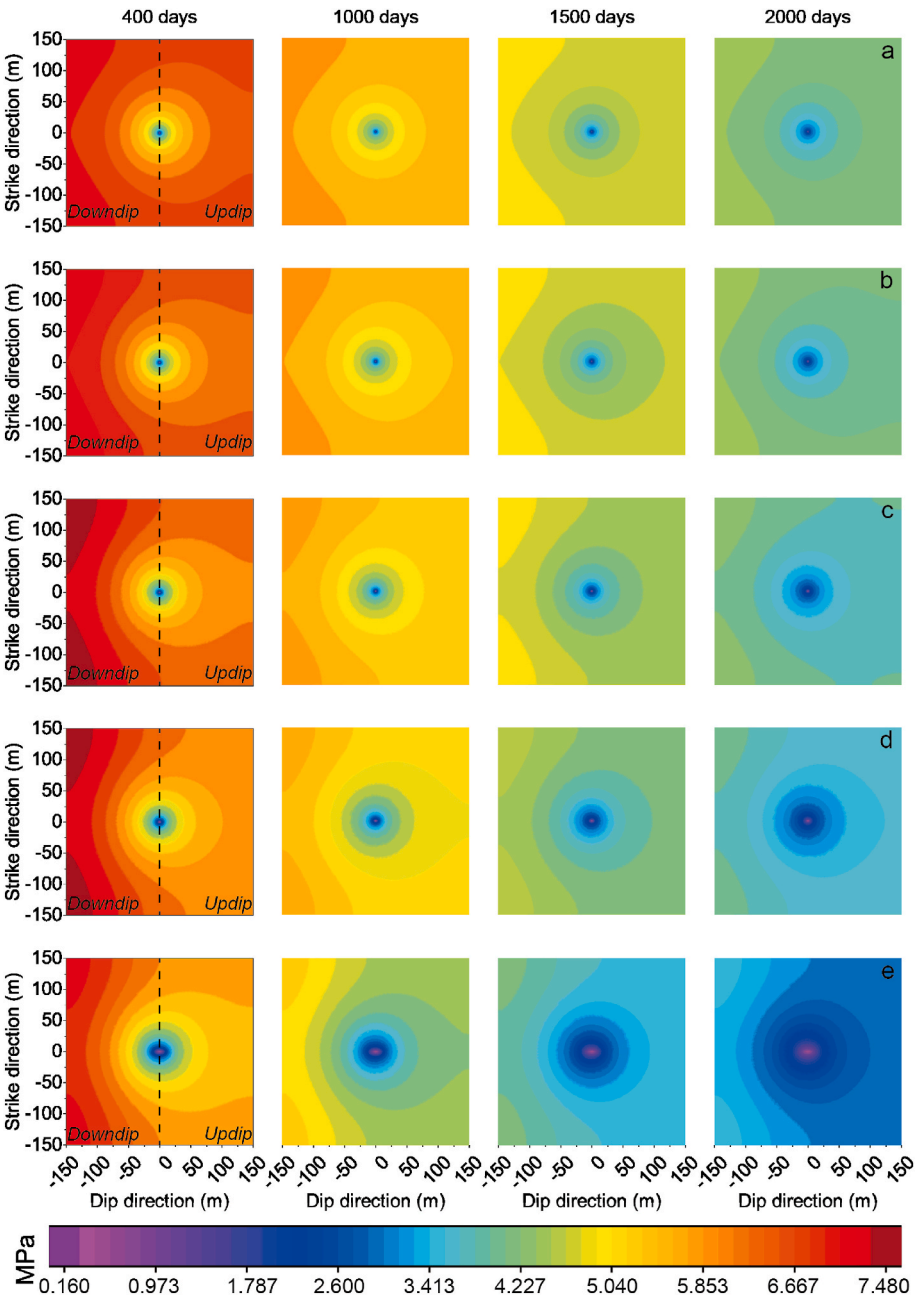

Fig. 8. Reservoir pressures for seams with various inclinations (a-15°, b-30°, c-45°, d-60°, e–75°) from production day 400–2000.

drop due to continuing drainage and gas desorption. As the seam inclination increases, the pressure drops in both updip and downdip reservoirs tend to become more pronounced as drainage and gas production proceed (Table 7 and Table 8). A statistical analysis reveals that at a location 50 m away from the production well, the pressure drops in the updip reservoirs (at measuring point 2) at inclinations of 15°, 30°, 45°, and 60° first increase and then decrease. The pressure drop in the updip reservoir (at measuring point 2) at an inclination of 75° consistently reduces with gas production. However, pressure drops in the downdip reservoirs (at measuring point 3) at varying inclinations (15°–75°) all decrease as gas production continues. The maximum pressure drops in both updip (at measuring point 2) and downdip reservoirs (at measuring point 3) are observed for the 75° inclined seam, which are individually 21.1% and 27.1% (Table 7). The pressure drops in both updip and downdip reservoirs with different dip angles at a location 100 m from the production well (measuring points 1 and 4) exhibit a similar evolutionary trend as those 50 m from the well (measuring points 2 and 3). Overall, the largest pressure drops in the updip and downdip reservoirs are 22.3% and 23.9% respectively (Table 8).

3.3. Evolution of gas content in reservoirs with various inclinations

The evolution of gas content in reservoirs with different dip angles also exhibits different degrees of asymmetry at symmetrical positions in the updip and downdip reservoirs relative to the production well. This is clearly different from the symmetrical evolution of gas content in horizontal reservoirs around the production well. For a seam with a smaller inclination (15°), limited variances exist in the initial reservoir pressure, permeability and other fluid parameters between the updip and downdip reservoirs, resulting in an approximate symmetrical distribution and evolution of gas content in the initial drainage stage with regard to the

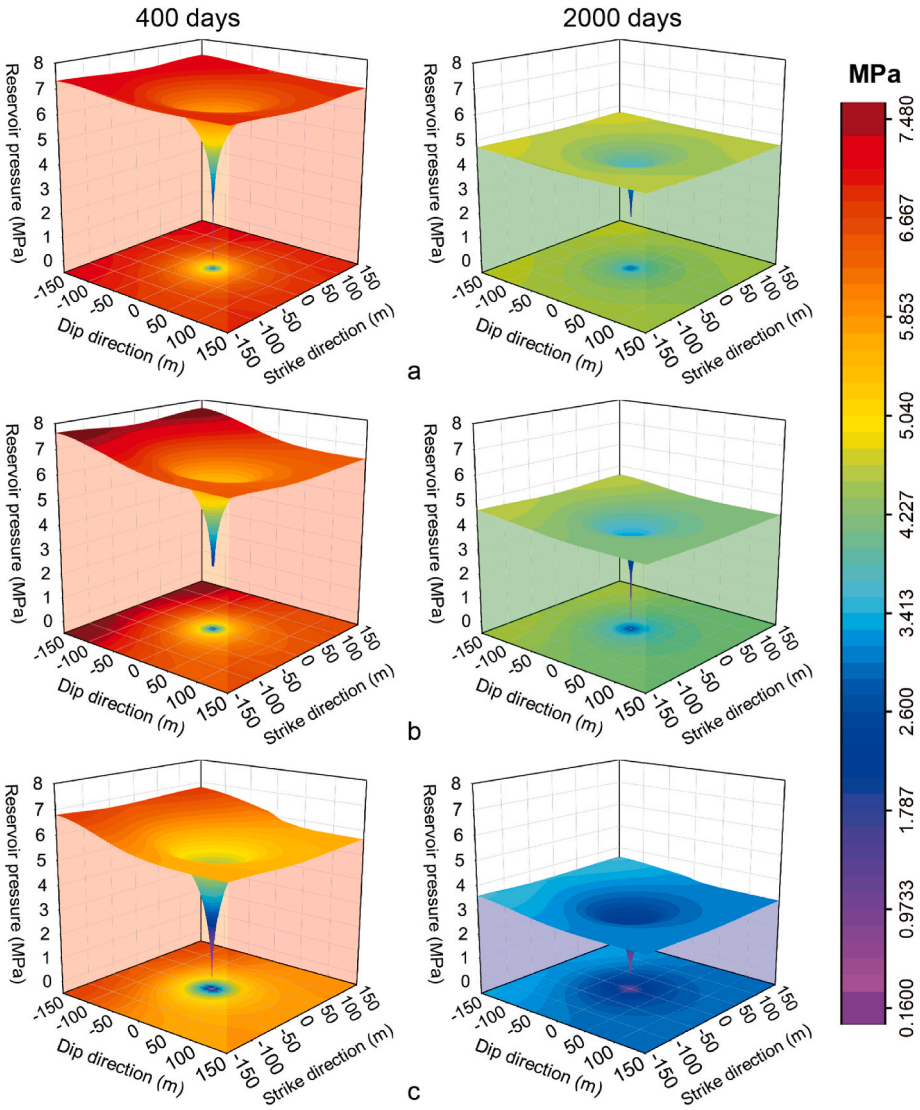

Fig. 9. Changes in reservoir pressure for seams with varying inclinations (a-15°, b-45°, c-75°) from production day 400–2000.

well. However, for a steeply inclined seam (e.g. ≥45°), the stress gradient increases within the reservoir, resulting in a more severe separation of gas and water. Physical properties of the reservoir also change more rapidly along the dip, resulting in a more distinctly asymmetric distribution of gas content relative to the well (Fig. 11).

3.4. Evolution of methane production and model validation

Reservoirs with various inclinations are characterized by different initial mechanical properties and permeabilities. This results in differences in the evolution of reservoir pressure, gas content and permeability, and eventually methane production. The cumulative methane production of seams with different dip angles is listed in Fig. 12. When the inclination increases from 15° to 75°, the cumulative CH_4 production (on production day 2200) grows from 3.04×10^6 m^3 to 4.98×10^6 m^3, up by 63.8%, indicating that a greater dip angle facilitates the drainage of the reservoir, and is beneficial to gas desorption and production.

The daily gas production follows the overall trend of first decreasing then increasing - then as drainage continues, the daily production starts to slowly drop (Fig. 13). The daily gas production accordingly increases as the seam dip angle increases, which of a seam at an inclination of 75° is approximately 1–2 times that of a seam at other small inclinations (<75°). Moreover, as the dip angle increases, the daily production rebound arises later. It is worth noting that when the dip angle is less than 45°, there is only one single peak on the daily gas production profile. However, when the inclination is ≥ 45°, as water drainage and gas production proceed, the speed of daily gas production decline slows down. We define this segment curve with a smaller rate of decline on the daily gas production profile as the second peak (as indicated by the red dashed arrow in Fig. 13). That is, the "dual-peak" emerges on the production profile of a reservoir with an inclination ≥45°. After reaching the second peak, the daily gas production continues to decline slowly. It is believed that this characteristic of "dual-peak" in the evolution of gas production for steeply inclined reservoirs real exists. Because the similar and more distinct feature has been observed on the actual gas production profiles from the well group 15 (Fig. 14a) and other 8 wells (multi-layer: CSD03, CSD04, CSD05, CS11-X2, and CSP06–1V; single layer: CSD01, CSD02, and CS11-X1) (Figs. 14b),[34] which are distributed in the Badaowan Formation of the west Fukang Block on the southern margin of the Junggar Basin. The dip angle of reservoirs there is generally greater than 50°.

As shown in Figs. 13 and 14, the time gaps between the dual peaks on the observed gas production profiles (Fig. 14) are obviously discrete due to the complex on-site geological conditions, while are not discrete for those time gaps on production profiles from numerical simulation (Fig. 13). The appearance of the dual peaks tends to move forward in

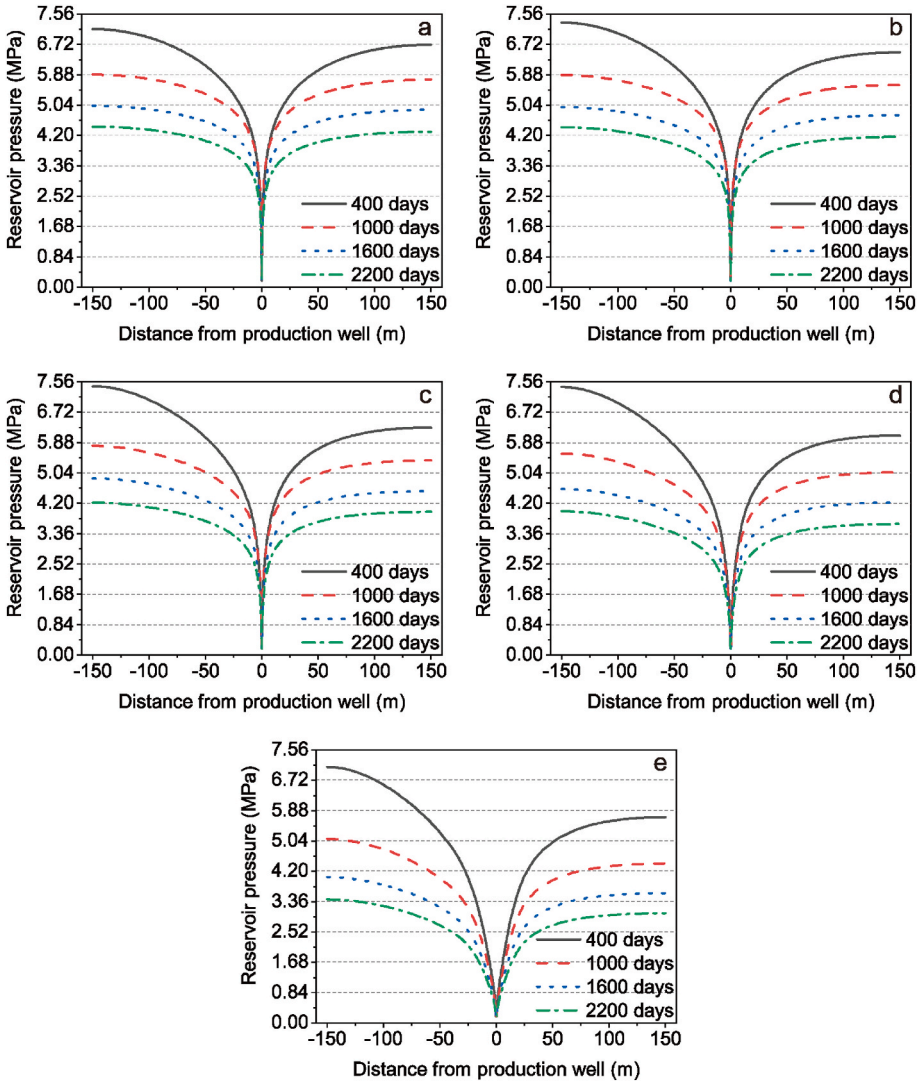

Fig. 10. Distribution of reservoir pressure around the well along the central dip direction for seams with varying inclinations (a-15°, b-30°, c-45°, d-60°, e−75°) from production day 400–2200.

Table 7
Pressure drops corresponding to seams with different inclinations after different production periods (at a location 50 m away from the production well, measuring points 2 (updip) and 3 (downdip)).

Production time (day)	Updip/ Downdip	The dip angle of the reservoir				
		15°	30°	45°	60°	75°
400–1000	Updip	11.3%	11.3%	12.3%	15.0%	**21.1%**
	Downdip	16.6%	18.5%	20.6%	23.2%	**27.1%**
1000–1600	Updip	14.1%	14.6%	15.5%	16.4%	18.8%
	Downdip	14.5%	15.0%	15.5%	17.3%	20.5%
1600–2200	Updip	12.2%	12.5%	12.7%	14.1%	15.7%
	Downdip	11.5%	11.3%	13.6%	13.5%	15.3%

Table 8
Pressure drops corresponding to seams with different inclinations after different production periods (at site 100 m away from the production well, measuring points 1 (updip) and 4 (downdip)).

Production time (day)	Updip/ Downdip	The dip angle of the reservoir				
		15°	30°	45°	60°	75°
400–1000	Updip	13.8%	13.4%	14.1%	16.5%	**22.3%**
	Downdip	12.8%	14.1%	16.1%	18.5%	**23.9%**
1000–1600	Updip	14.4%	14.8%	15.7%	16.5%	18.6%
	Downdip	14.2%	14.6%	15.4%	16.9%	20.0%
1600–2200	Updip	12.4%	12.7%	12.6%	14.1%	15.6%
	Downdip	11.7%	11.6%	13.2%	13.8%	15.7%

time as inclination increases, also resulting in a shorter time gap between the twin peaks (Fig. 13). Specifically, the gaps between these two peaks are 1194 days, 975 days, and 818 days corresponding to seams at inclinations of 45°, 60°, and 75°respectively. It's surmised that the water drainage decays in the updip reservoir prior to that in the downdip reservoir, and it is the same for gas desorption between the updip and downdip reservoirs. Therefor both the dual peaks emerge earlier and forms a shorter time gap for seams with larger dip angles. Both the daily gas productions of the well group 15 and other 8 wells (average daily production) observed on-site are larger compared with that of a single well in the numerical simulation. The peak daily gas production from the simulation is ~1800–3000 m^3/d. While the peak daily gas production of well group 15 and other 8 wells (average daily production) are approximately 7000–8000 m^3/d and 6000–8000 m^3/d, respectively. This is speculated reasonable since the former came from a single well in one single inclined reservoir, but the latter came from the well group and a well penetrating multi layers. Above analysis also indirectly proves the rationality of the model, indicating that the model is effective

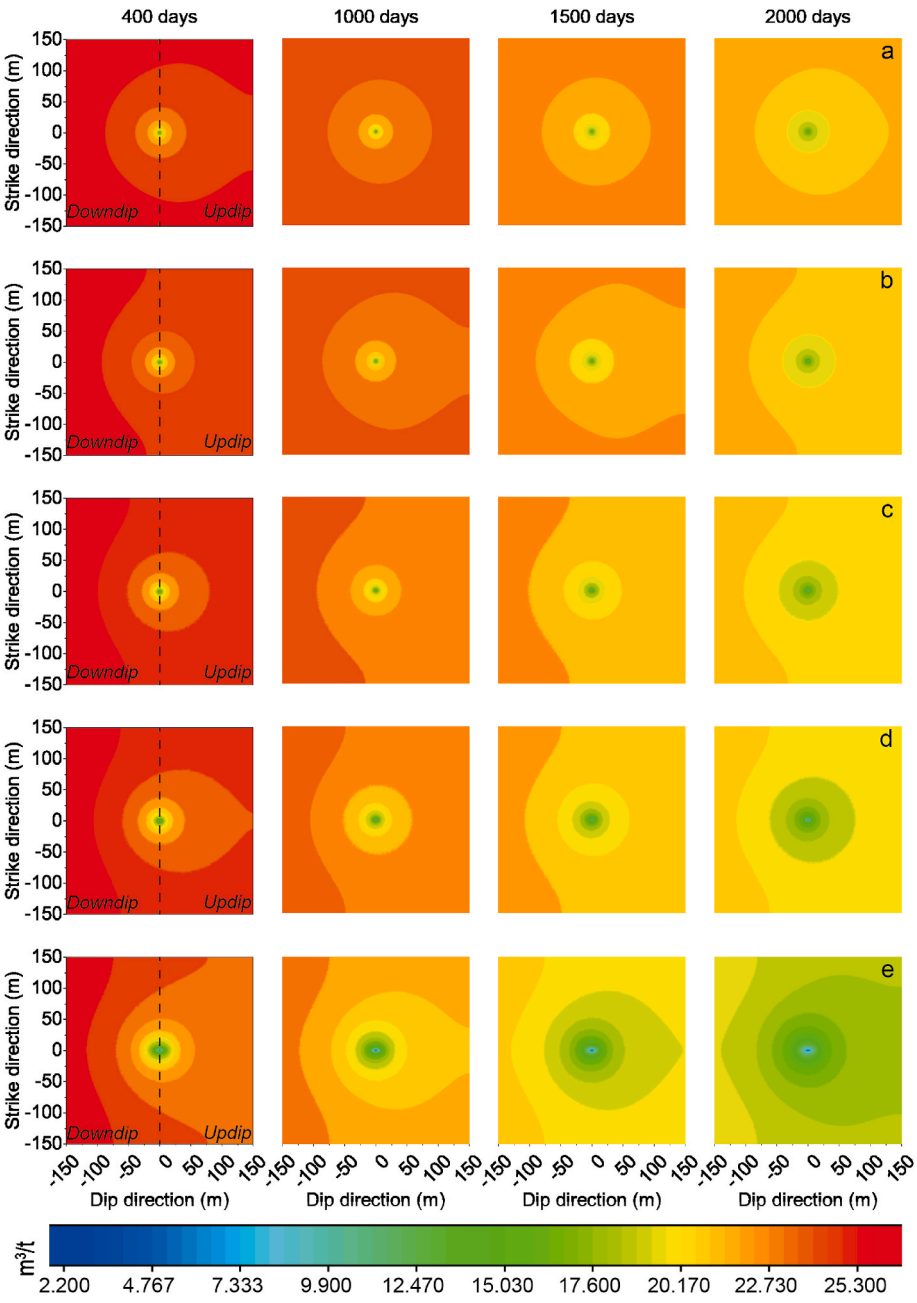

Fig. 11. Methane content corresponding to inclined seams with various inclinations (a-15°, b-30°, c-45°, d-60°, e−75°).

for examining the CBM development in steeply inclined reservoirs.

The occurrence of dual peaks on the daily gas production profile is mainly attributed to the increasing differences in permeability and reservoir pressures between the updip and downdip reservoirs with growing inclination. In Fig. 13, during stage I of gas production (early stage), the fluid pressure drops and the effective stress gradually increases as the water and gas are drained from both the updip and downdip reservoirs. This results in the dominance of effective stress on permeability evolution. The pores within the matrix compact, reducing permeability in both the updip and downdip reservoirs, eventually resulting in reduced methane production. In stage I, methane mainly comes from the updip reservoir. During stage II of gas production (mid-stage), when the updip reservoir pressure drops to the threshold of gas desorption and change in permeability is dominated by gas desorption. However, the downdip reservoir is still within the main drainage stage, resulting in a greater permeability difference which triggers the rebound of methane production. In addition, gas production increases with reservoir inclination and the updip reservoir contributes more methane. During stage III (late stage), as the intensive drainage of the downdip reservoir ends, both the updip and downdip reservoirs contribute to methane production, resulting in the emergence of the second peak of gas production. During stage III, the methane production is mainly contributed by the downdip reservoir.

According to the foregoing analysis, the steeply-inclined reservoir results in large differences in physical properties of the shallow updip reservoir and deep downdip reservoir, especially the permeability, reservoir pressure, and gas content. These changes cause the unsynchronized desorption of methane in the updip and downdip reservoirs. It is inferred that methane in the updip reservoir desorbs preferentially over that in the downdip reservoir. The time gap in gas desorption between the updip and downdip reservoirs results in the “dual-peak” on the production profile. The first daily production peak is mainly caused

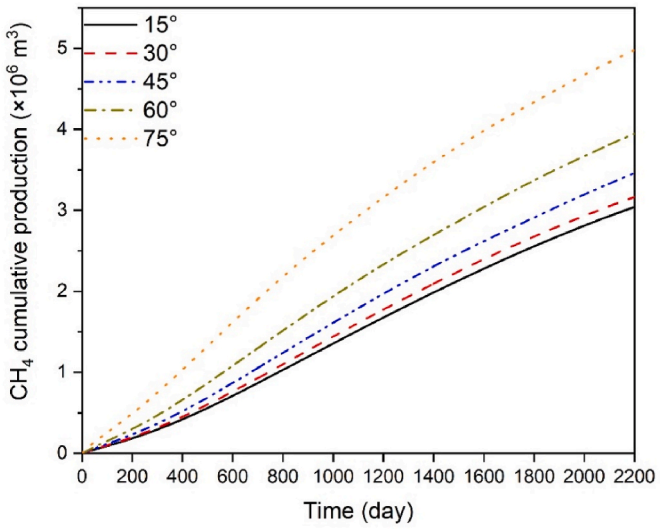

Fig. 12. Cumulative CH_4 production for seams with various inclinations.

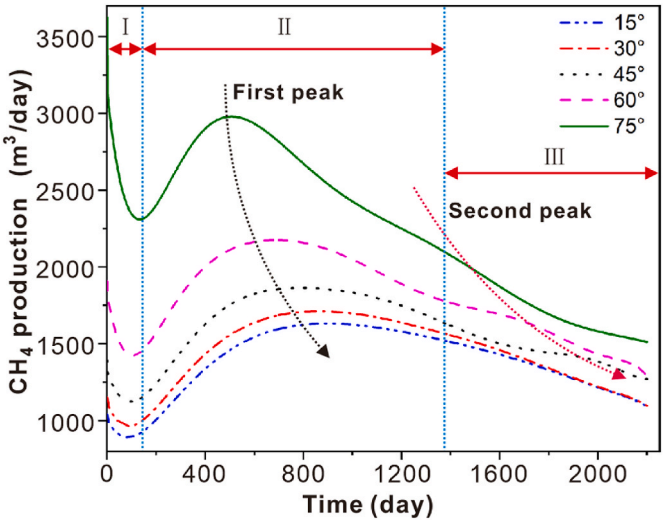

Fig. 13. Methane production profiles for seams with various inclinations.

by methane desorption in the updip reservoir, and methane desorption in the downdip reservoir contributed more to the second production peak.

4. Discussion

This work follows from Kang et al.[13] and adds hydro-mechanical coupling to accommodate the effects of water and gas (the buoyancy and gravity) for steeply inclined reservoirs. The field case was used to verify the accuracy of the numerical simulation results. With this model, we have investigated the temporal and spatial evolution of permeability, pressure, gas content, and methane production during the process of water drainage and gas extraction in reservoirs with various inclinations. This study identifies the variance in permeability and methane production and provides insights into well-type selection and layouts in such steeply dipping seams (~50°–85°) common within the Junggar Basin of Xinjiang Province.

4.1. Comparison with previous studies

Many studies have been conducted to probe permeability evolution

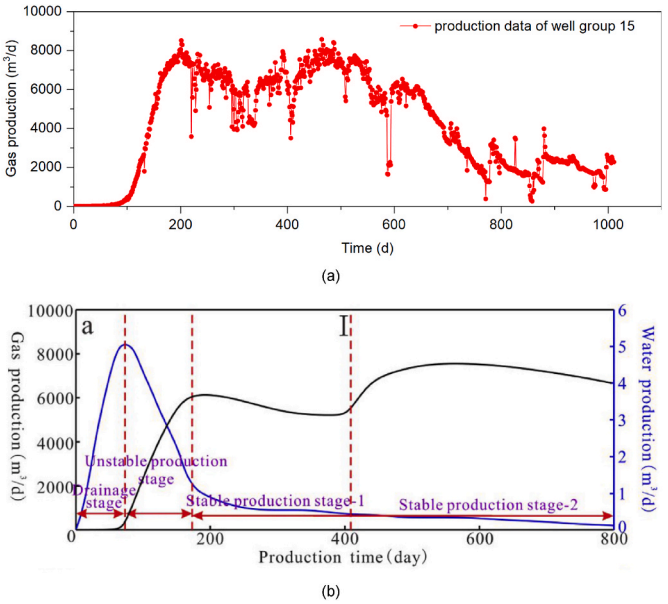

Fig. 14. Methane production profile of well group 15 (a) and the average methane production profile of 8 wells (b)[34] that distributed in the Badaowan Formation of the west Fukang Block on the southern margin of the Junggar Basin, Xinjiang, China.

and to promote the development of CBM. However, these studies are mainly aimed at horizontal or slightly inclined reservoirs according to the field geological conditions.[3,4,19–22,24,37–39] Even inclined seams with a dip angle around 15° are also assumed to be horizontal layers for simplicity.[19,32] This is inappropriate, especially for steeply inclined reservoirs (> 45°) on the southern margin of the Junggar Basin, China, in which the migration of gas and water significantly differs much from that in horizontal coal seams due to the stress gradient and buoyancy of both gas and water. Taking the seam with a dip angle of 45° as an example, for an inclined 300 m × 300 m square area, the burial depth difference is 212 m between the upper and lower boundaries of the seam. This obviously impacts the initial physical parameters of the reservoir, which has been accommodated in our model. We reproduced the "deal-peak" characteristic of gas production profiles of steeply inclined reservoirs through discrete and finite element numerical simulation. The mechanism of this characteristic has been revealed through analyzing the spatiotemporal evolution of permeability and reservoir pressure in both the updip and downdip reservoirs. Besides, the literature 27, 28, and 35 qualitatively reported the characteristic of "gas--water separation" in the process of water drainage and gas production in steeply-dipping reservoirs. However, they omitted the influence of initial physical parameters of the reservoir, and rigorous mathematical analysis on the hydro-mechanical coupling effects is absent.

We explain the various impacts of gravity on permeability in both the updip and downdip parts of the reservoir with different inclinations by analyzing the drawdown and recovery times of permeability and the permeability differences in the updip and downdip reservoirs. With increasing inclination, the permeability difference between the updip and downdip reservoirs correspondingly amplifies. Previous studies have indicated that a greater inclination could result in greater pressure difference between the updip and downdip reservoirs,[66] however, the rate of pressure drop across the entire reservoir has not been previously analyzed. This study indicates that when it is far from the production well, the pressure drop in the updip region of a shallow (<45°) reservoir tends to first increase then decrease as drainage and then gas production proceed. Conversely, the pressure drop tends to decrease continuously for steep seams (>45°). This results in a single peak in CH_4 production for shallow seams (<45°) but dual peaks for steep seams (>45°). We

surmise that this results from different contributions of the updip and downdip reservoirs in methane production under the influence of the deviatoric stress depending on the reservoir dip.

4.2. Well pattern optimization for steeply inclined reservoirs

In terms of the well layout, rectangular four-point well patterns are often adopted for horizontal or slightly inclined reservoirs. Reasonable spacings between neighboring wells are typically selected independent of reservoir dip angles. However, for steep reservoirs, the stress gradient resulting from gravity tends to dominate. The dip facilitates water transport and obstructs the gas from migrating to the drainage well within the updip part of the reservoir. The reverse effect is exerted on the water and gas within the downdip part of the reservoir. A larger well spacing along the dip of a more highly inclined reservoir results in more efficient water drainage and gas production. Often a greater burial depth leads to a lower initial permeability. The difference in permeability between the updip and downdip reservoirs within the influence range of a single well tends to be more distinct as the inclination increases. In addition, due to the asymmetric form of the pressure drop, this permeability difference also intensifies with the drainage process, which in turn exerts further impact on pressure drop and methane migration within the reservoirs. That is, methane productivity of a single well located in the updip reservoir is larger than that of a well in the downdip reservoir. The along-strike well spacing could be smaller for wells located in the downdip reservoir. Therefore, an inverted trapezoidal well pattern is recommended to facilitate the drainage and gas production of reservoirs with significant dip angles. In this way, the along-strike well spacing in the updip reservoir (a_i) is greater than that in the downdip reservoir (b_i) (Fig. 15). Thus, the well spacing along-dip (c_i) will increase correspondingly as the seam dip angle increases (Fig. 15). This recommendation is actually consistent with Ni et al.'s work.[72] The inverted trapezoidal well pattern is proposed for CBM development in the anticline and syncline of the reservoir, which are inclined.

4.3. Shortcomings and prospect

Although we investigate the evolution of pressure, permeability and methane production in inclined reservoirs across a spectrum of dip angles (15°, 30°, 45°, 60°, and 75°), our coupled model is hampered by assumptions that the elastic modulus and other deformation parameters in the reservoir are constant during drainage and gas production. Experimental studies have shown that as the bedding inclination in the coal sample increases, the initial permeability declines due to the anisotropy of the coal sample.[10,67,68] It has been confirmed that the horizontal permeability is often larger than that in the direction of the vertical bedding planes according to the field and laboratory study,[67,71] and the max ratio of permeability in different directions of coal bedding plane could be 17:1.[69–71] In addition, coal samples with different bedding angles also have different strength and deformation characteristics. Therefore, in order to more accurately investigate the evolution of permeability, reservoir pressure, and productivity of reservoirs with different dip angles, some subsequent work is needed. Firstly, for steeply inclined coal seams, permeability anisotropy plays an important role in determining the behavior of gas-water two-phase flow and assessing CBM productivity, which requires further study. Secondly, the relationship between coal stiffness and burial depth needs to be quantified in an improved model and must be included in the numerical calculation as initial parameters. Thirdly, changes in the fluid system within the reservoir due to water drainage could not only directly exert impact on coal mass stiffness and result in additional matrix deformation but also indirectly affect the reservoir stiffness and change the resulting geo-stress condition. Thus, future refinements include the need of an improved permeability coupling model involving the temporal and spatial evolution of the reservoir fluid system and geo-stress environment.

5. Conclusions

(1) The difference in the permeability ratio between the updip and downdip reservoirs intensifies with increasing dip angle. A greater reservoir inclination is more beneficial to gravity drainage in the updip reservoir, resulting in greater permeability difference within the updip reservoir. The permeability difference decreases as drainage and gas production proceeds in the updip reservoir, but increases with drainage and gas production in the downdip reservoir. However, the permeability difference in the entire reservoir also increases as gas production proceeds, indicating that the permeability changes more intensely in the downdip reservoir, which then dominates the permeability evolution of the entire reservoir.

(2) An apparent asymmetric distribution of reservoir pressures is identified for wells along-dip. The difference in reservoir pressure between the updip and downdip reservoirs intensifies as the dip angle increases, but lessens as drainage proceeds - the larger the seam dip angle, the smaller the final reservoir pressure. Due to the strengthening and weakening effects of gravity on dewatering within the updip and downdip reservoirs, respectively, the reservoir pressures of both the updip and downdip reservoirs decline rapidly in the initial stage of drainage. Following this, pressures fall slowly. Pressure reduction in the downdip reservoir is larger than that in the updip reservoir. However, reservoir pressure within the downdip limb of the seam is always larger than that within the updip limb.

(3) The evolution of gas content in reservoirs with different dip angles also exhibits different degrees of asymmetry at symmetrical locations in the updip and downdip reservoirs, which is clearly different from the symmetrical evolution of gas content in horizontal reservoirs. A steeper inclination leads to a higher CH_4 production rate. Gas production rate in a reservoir with an inclination of 75° is approximately 1–2 times that of a reservoir with a dip angle less than 60°. When the dip angle is < 45°, only a single peak in methane production rate exists and this transforms to twin-peaks as dip gradually increases from 45° to 75°. The occurrence of these twin-peaks is accelerated as the reservoir dip angle increases. The "dual-peak" feature has been observed from the daily gas production profiles of well group 15 and other 8 wells located in the west Fukang Block on the southern margin of

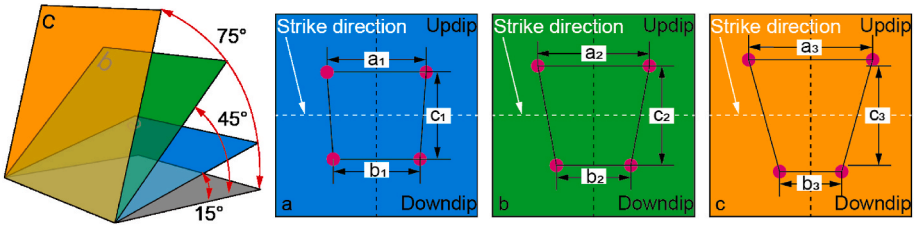

Fig. 15. Suggested optimal well patterns for reservoirs with various inclinations (15°, 45°, and 75°). a_i and b_i indicate the well spacing along the strike in the updip and downdip reservoirs, respectively. c_i indicates the well spacing along the dip between the updip and downdip reservoirs ($a_3>a_2>a_1\geq b1>b_2>b_3$, $c_3>c_2>c_1$).

the Junggar Basin, Xinjiang Province. This validates the rationality of the model.

(4) The steeply-inclined reservoir results in large differences in physical properties of the updip reservoir and downdip reservoir, especially the permeability, reservoir pressure, and gas content. These changes cause the unsynchronized desorption of methane in the updip and downdip reservoirs. Methane in the updip reservoir desorbs preferentially over that in the downdip reservoir. The time gap in gas desorption between the updip and downdip reservoirs results in the "dual-peak" on the production profile. The first daily production peak mainly results from methane desorption in the updip reservoir, and methane desorption in the downdip reservoir contributed more to the second production peak.

(5) A larger well spacing along the dip of a more highly inclined reservoir results in more efficient water drainage and gas production. Due to the asymmetric evolution of permeability, reservoir pressure and gas content, methane productivity of a single well located in the updip reservoir is larger than that of a well in the downdip reservoir. Thus, an inverted trapezoidal well pattern is recommended to facilitate the drainage and gas production of reservoirs with significant dip angles. The along-strike well spacing in the updip reservoir is greater than that in the downdip reservoir. The well spacing along-dip increases correspondingly as the seam dip angle grows.

Declaration of competing interest

The authors declare that they have no known competing financial interests or personal relationships that could have appeared to influence the work reported in this paper.

Data availability

Data will be made available on request.

Acknowledgment

Financial support for this work, provided by the National Natural Science Foundation of China (No. 52174139, 41602174, 42202198), the Assistance Program for Future Outstanding Talents of China University of Mining and Technology (2020WLJCRCZL095), and the Priority Academic Program Development of Jiangsu Higher Education Institutions (PAPD), is gratefully acknowledged. Derek Elsworth acknowledges support from the G. Albert Shoemaker endowment.

Nomenclature

ε_{ki}	strain tensor
G	shear modulus
D	effective elastic modulus
E	Young's modulus of the coal
ν	Poisson's ratio of coal
σ_{ki}	component of the total stress tensor
σ_{ll}	normal stress component
K	bulk modulus of the coal
K_S	bulk modulus of the coal grains
L_m	the width of the matrix
L_f	the aperture of fracture
K_n	normal stiffness of fracture
K_f	modified fracture stiffness
ε_s	volume strain within the matrix
ε_l	Langmuir-type strain coefficient
p_l	Langmuir gas pressure constant
p_m	gas pressure in the matrix
δ_{ki}	Kronecker delta, 1 for k = i and 0 for k≠i
α_m	Biot effective stress coefficient for the matrix
α_f	Biot effective stress coefficient for the fracture network
p_{mg}	gas pressure in the matrix
p_{fg}	gas pressure in the fractures
p_{fw}	water pressure in the fractures
p_f	the total fluid pressure within the fractures
s_w	water phase saturation, $S_g + S_w = 1$
s_g	gas phase saturation
p_c	pumping negative pressure
u_k	displacement in the k-direction
F_k	body force in the k-direction
m_g	mass of gas in the matrix
M_g	molar mass of methane
R	the molar constant of methane
T	temperature of coal reservoir
D_i	gas diffusion coefficient
L	cleat spacing
ρ_s	density of the coal matrix
T_s	reservoir temperature under standard conditions
p_s	standard atmospheric pressure

V_L	Langmuir volume constant
P_L	Langmuir pressure constant
φ_m	porosity of coal matrix
φ_f	fracture porosity of coal
b	Klinkenberg factor
k_f	fracture permeability of the coal
k_{rg}	the relative permeability of gas
k_{rw}	the relative permeability of water
μ_g	gas dynamic viscosity
μ_w	water dynamic viscosity
ρ_g	gas density
ρ_w	water density
ρ_c	coal density
ρ_r	rock density
∇z	the gravitational term
s_{wr}	irreducible water saturation
s_{gr}	residual gas saturation
$\Delta\varepsilon_s$	swelling strain of coal mass
$\Delta\varepsilon_v$	volumetric strain of coal mass

subscript

0	initial value of the variable
m	matrix
f	fracture

References

1 Dai J. Coal-derived gas theory and its discrimination. *Chin Sci Bull*. 2018;63(14):1290–1305.
2 Guan C, Li C, Wang Y, Zhao Y. The temperature effect on the methane and CO_2 adsorption capacities of Illinois coal. *Fuel*. 2017;211:241–250.
3 Wang L, Chen Z, Wang C, Elsworth D, Liu W. Reassessment of coal permeability evolution using steady-state flow methods: the role of flow regime transition. *Int J Coal Geol*. 2019;211, 103210.
4 Song H, Lin B, Zhong Z, Liu T. Dynamic evolution of gas flow during coalbed methane recovery to reduce greenhouse gas emission: a case study. *ACS Omega*. 2022;7(33):29211–29222.
5 Wolde-Rufael Y. Coal consumption and economic growth revisited. *Appl Energy*. 2010;87(1):160–167.
6 Aydin G, Karakurt I, Aydiner K. Evaluation of geologic storage options of CO_2: applicability, cost, storage capacity and safety. *Energy Pol*. 2010;38(9):5072–5080.
7 Aydin G. The application of trend analysis for coal demand modeling. *Energy Sources B Energy Econ Plann*. 2015;10(2):183–191.
8 Aydin G, Jang H, Topal E. Energy consumption modeling using artificial neural networks: the case of the world's highest consumers. *Energy Sources B Energy Econ Plann*. 2016;11(3):212–219.
9 Wan Y, Liu Y, Ouyang W, Liu W, Han G. Desorption area and pressure-drop region of wells in a homogeneous coalbed. *J Nat Gas Sci Eng*. 2016;28:1–14.
10 Zhang T, Tao S, Tang D, et al. Permeability anisotropy in high dip angle coal seam: a case study of southern Junggar Basin. *Nat Resour Res*. 2021;30(3):2273–2286.
11 Zhang C, Zhu D, Luo Q, et al. Major factors controlling fracture development in the Middle Permian Lucaogou Formation tight oil reservoir, Junggar Basin, NW China. *J Asian Earth Sci*. 2017;146:279–295.
12 Tao S, Pan Z, Tang S, Chen S. Current status and geological conditions for the applicability of CBM drilling technologies in China: a review. *Int J Coal Geol*. 2019;202:95–108.
13 Kang J, Fu X, Liang S, Li X, Chen X, Wang Z. A numerical simulation study on the characteristics of the gas production profile and its formation mechanisms for different dip angles in coal reservoirs. *J Petrol Sci Eng*. 2019;181, 106198.
14 Han H, Liang S, Liang Y, et al. The role of coal mechanical characteristics on reservoir permeability evolution and its effects on CO_2 sequestration and enhanced coalbed methane recovery. *Geofluids*. 2020;2020:1–28.
15 Liang S, Han H, Elsworth D, et al. Evolution of production and transport characteristics of steeply-dipping ultra-thick coalbed methane reservoirs. *Energies*. 2020;13(19):5081.
16 Luo X, Wang Z, Zhang L, Yang W, Liu L. Overpressure generation and evolution in a compressional tectonic setting, the southern margin of Junggar Basin, northwestern China. *AAPG Bull*. 2007;91(8):1123–1139.
17 Fu H, Tang D, Xu T, et al. Preliminary research on CBM enrichment models of low-rank coal and its geological controls: a case study in the middle of the southern Junggar Basin, NW China. *Mar Petrol Geol*. 2017;83:97–110.
18 Li X, Fu X, Liu A, et al. Methane adsorption characteristics and adsorbed gas content of low-rank coal in China. *Energy Fuel*. 2016;30(5):3840–3848.
19 Li S, Tang D, Pan Z, Hao X, Ren P. Geological conditions of deep coalbed methane in the eastern margin of the Ordos Basin, China: implications for coalbed methane development. *J Nat Gas Sci Eng*. 2018;53:394–402.
20 Huo B, Jing X, He A, Fan C. Hydraulic-mechanical coupling model with dual-porosity dual-permeability for anisotropy coal seams and its application in mine gas extraction. *Adv Civ Eng*. 2019;2019:1–12.
21 Li S, Fan C, Han J, Luo M, Yang Z, Bi H. A fully coupled thermal-hydraulic-mechanical model with two-phase flow for coalbed methane extraction. *J Nat Gas Sci Eng*. 2016;33:324–336.
22 Fan C, Elsworth D, Li S, Zhou L, Yang Z, Song Y. Thermo-hydro-mechanical-chemical couplings controlling CH_4 production and CO_2 sequestration in enhanced coalbed methane recovery. *Energy*. 2019;173:1054–1077.
23 Fan C, Yang L, Sun H, et al. Recent advances and perspectives of CO_2-enhanced coalbed methane: experimental, modeling, and technological development. *Energy Fuel*. 2023;37(5):3371–3412.
24 Fan C, Luo M, Li S, Zhang H, Yang Z, Liu Z. A Thermo-hydro-mechanical-chemical coupling model and its application in acid fracturing enhanced coalbed methane recovery simulation. *Energies*. 2019;12(4):626.
25 Keim SA, Luxbacher KD, Karmis M. A numerical study on optimization of multilateral horizontal wellbore patterns for coalbed methane production in Southern Shanxi Province, China. *Int J Coal Geol*. 2011;86(4):306–317.
26 Sun Z, Li X, Shi J, et al. A semi-analytical model for drainage and desorption area expansion during coal-bed methane production. *Fuel*. 2017;204:214–226.
27 Jiang R, Wang Y, Li H, Yang M. A numerical simulation on the impact of coal seam dip on productivity of CBM horizontal well. *J China Coal Soc*. 2015;40(4):151–157 (S1).
28 Wang C, Peng X, Zhu S, Sun H, Zhang J, Lin L. Coalbed methane well-type optimization and well pattern arrangement for thick coal seam with a large dip angle. *Chin J Rock Mech Eng*. 2019;38(2):313–320.
29 Zhang J, Bai M, Roegiers JC, Wang J, Liu T. Experimental determination of stress permeability relationship. *Pacific Rock*. 2000:817–822, 2000.
30 Mastalerz M, Drobniak A, Strąpoć D, Solano Acosta W, Rupp J. Variations in pore characteristics in high volatile bituminous coals: implications for coal bed gas content. *Int J Coal Geol*. 2008;76(3):205–216.
31 Rutqvist J. Fractured rock stress-permeability relationships from in situ data and effects of temperature and chemical-mechanical couplings. *Geofluids*. 2015;15(1-2):48–66.
32 Xu H, Tang D, Tang S, et al. Geologic and hydrological controls on coal reservoir water production in marine coal-bearing strata: a case study of the Carboniferous Taiyuan Formation in the Liulin area, eastern Ordos Basin, China. *Mar Petrol Geol*. 2015;59:517–526.
33 Fu X, Kang J, Liang S, Gao L, Chen X. Well type optimization and physical property in gas drainage process of steep inclined coal reservoir in Fukang Western Block. *Coal Sci Technol*. 2018;46(6):9–16.
34 Kang J, Fu X, Gao L, Liang S. Production profile characteristics of large dip angle coal reservoir and its impact on coalbed methane production: a case study on the Fukang west block, southern Junggar Basin, China. *J Petrol Sci Eng*. 2018;171:99–114.
35 Wang S, Wang F, Hou G, et al. CBM development well type for steep seam in Fukang Baiyanghe mining area, Xinjiang. *J China Coal Soc*. 2014;39(9):1914–1918.

36 Fan C, Li S, Luo M, Yang Z, Zhang H, Wang S. Deep CBM extraction numerical simulation based on hydraulic-mechanical thermal coupled model. *J China Coal Soc*. 2016;41(12):3076–3085.
37 Zhu W, Liu J, Sheng JC, Elsworth D. Analysis of coupled gas flow and deformation process with desorption and Klinkenberg effects in coal seams. *Int J Rock Mech Min*. 2007;44(7):971–980.
38 Dong J, Cheng Y, Jin K, et al. Effects of diffusion and suction negative pressure on coalbed methane extraction and a new measure to increase the methane utilization rate. *Fuel*. 2017;197:70–81.
39 Liu J, Chen Z, Elsworth D, Miao X, Mao X. Linking gas-sorption induced changes in coal permeability to directional strains through a modulus reduction ratio. *Int J Coal Geol*. 2010;83(1):21–30.
40 Palmer I, Mansoori J. How permeability depends on stress and pore pressure in coalbeds: a new model. *SPE Reservoir Eval Eng*. 1998;1(6):539–544.
41 Chen Z, Liu J, Elsworth D, Connell LD, Pan Z. Impact of CO_2 injection and differential deformation on CO_2 injectivity under in-situ stress conditions. *Int J Coal Geol*. 2010;81(2):97–108.
42 Khalili N. Two-phase fluid flow through fractured porous media with deformable matrix. *Water Resour Res*. 2008;44(5):1–12.
43 Liu J, Chen Z, Elsworth D, Miao X, Mao X. Evaluation of stress-controlled coal swelling processes. *Int J Coal Geol*. 2010;83(4):446–455.
44 Zhu W, Wei C, Liu J, Qu H, Elsworth D. A model of coal-gas interaction under variable temperatures. *Int J Coal Geol*. 2011;86:213–221.
45 Fan Y, Deng C, Zhang X, Li F, Wang X, Qiao L. Numerical study of CO_2 -enhanced coalbed methane recovery. *Int J Greenh Gas Con*. 2018;76:12–23.
46 Shi JQ, Durucan S. Drawdown induced changes in permeability of coalbeds: a new interpretation of the reservoir response to primary recovery. *Transport Porous Media*. 2004;56:1–16.
47 Zhang HB, Liu J, Elsworth D. How sorption-induced matrix deformation affects gas flow in coal seams: a new FE model. *Int J Rock Mech Min*. 2008;45(8):1226–1236.
48 Harpalani S, Chen G. Influence of gas production induced volumetric strain on permeability of coal. *Geotech Geol Eng*. 1997;15(4):303–325.
49 Robertson EP, Christiansen RL. Modeling laboratory permeability in coal using sorption-induced-strain data. *SPE Reservoir Eval Eng*. 2007;10(3):260–269.
50 Xia T, Zhou F, Liu J, Hu S, Liu Y. A fully coupled coal deformation and compositional flow model for the control of the pre-mining coal seam gas extraction. *Int J Rock Mech Min*. 2014;72:138–148.
51 Biot MA. General theory of three-dimensional consolidation. *J Appl Phys*. 1941;12:155–164.
52 Salimzadeh S, Khalili N. Three-Dimensional numerical model for double-porosity media with two miscible fluids including geomechanical response. *Int J GeoMech*. 2016;16(3), 04015065.
53 Wu Y, Liu J, Elsworth D, Chen Z, Connell L, Pan Z. Dual poroelastic response of coal seam to CO_2 injection. *Int J Greenh Gas Con*. 2010;4:668–678.
54 Wang JG, Kabir A, Liu J, Chen Z. Effects of non-Darcy flow on the performance of coal seam gas wells. *Int J Coal Geol*. 2012;93:62–74.
55 Wang JG, Liu J, Kabir A. Combined effects of directional compaction, non-Darcy flow and anisotropic swelling on coal seam gas extraction. *Int J Coal Geol*. 2013;109–110:1–14.
56 Xia T, Zhou F, Gao F, Kang J, Liu J, Wang J. Simulation of coal self-heating processes in underground methane-rich coal seams. *Int J Coal Geol*. 2015;141–142:1–12.
57 Wu Y, Liu J, Elsworth D, Miao X, Mao X. Development of anisotropic permeability during coalbed methane production. *J Nat Gas Sci Eng*. 2010;2:197–210.
58 Xu H, Tang D, Tang S, Zhao J, Meng Y, Tao S. A dynamic prediction model for gas–water effective permeability based on coalbed methane production data. *Int J Coal Geol*. 2014;121:44–52.
59 Corey AT. The interrelation between gas and oil relative permeabilities. *Prod Mon*. 1954;19:38–41.
60 Liu J, Elsworth D. Three-dimensional effects of hydraulic conductivity enhancement and desaturation around mined panels. *Int J Rock Mech Min*. 1997;34(8):1139–1152.
61 Liu J, Elsworth D. Evaluation of pore water pressure fluctuation around an advancing longwall face. *Adv Water Resour*. 1999;22(6):633–644.
62 Xia T, Zhou F, Liu J, Gao F. Evaluation of the pre-drained coal seam gas quality. *Fuel*. 2014;130:296–305.
63 Cui X, Bustin RM. Volumetric strain associated with methane desorption and its impact on coalbed gas production from deep coal seams. *AAPG Bull*. 2005;89(9):1181–1202.
64 Liu J, Elsworth D, Brady BH. Linking stress-dependent effective porosity and hydraulic conductivity fields to RMR. *Int J Rock Mech Min*. 1999;36(5):581–596.
65 Liu J, Chen Z, Elsworth D, Qu H, Chen D. Interactions of multiple processes during CBM extraction: a critical review. *Int J Coal Geol*. 2011;87(3-4):175–189.
66 Ren J, Zhang L, Ren S, Lin J, Ren G, Meng S. Productivity analysis of different types wells in Liulin coalbed methane block. *J China Coal Soc*. 2015;40(S1):158–163.
67 Yan Z, Wang K, Zang J, Wang C, Liu A. Anisotropic coal permeability and its stress sensitivity. *Int J Min Sci Technol*. 2019;29(3):507–511.
68 Gash BW, Richard FV, Potter G, Corgan JM. The effects of cleat orientation and confining pressure on cleat porosity, permeability and relative permeability in coal. In: *Paper Presented at: SPWLA/SCA Symposium, Oklahoma City*. 1992.
69 Wang Z, Pan J, Hou Q, et al. Changes in the anisotropic permeability of low-rank coal under varying effective stress in Fukang mining area, China. *Fuel*. 2018;234:1481–1497.
70 Wang S, Elsworth D, Liu J. Permeability evolution in fractured coal: the roles of fracture geometry and water-content. *Int J Coal Geol*. 2011;87(1):13–25.
71 Koenig RA, Stubbs PB. Interference testing of a coalbed methane reservoir. In: *Paper Presented at: SPE Unconventional Gas Technology Symposium*. 1986.
72 Ni X, Wang Y, Jie M, Wu J. The relations between geological structure in the western Jincheng diggings and coal-bed methane wells arrangement. *J China Coal Soc*. 2007;32(2):146–149.